

This is to certify that the

thesis entitled

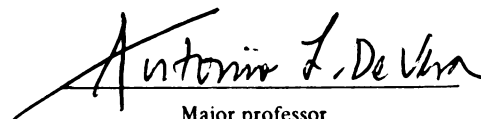
SOME KINETIC ASPECTS OF THE GASIFICATION
OF GRAPHITE AND PLATINUM GRAPHIMET

presented by

Seung I. Choi

has been accepted towards fulfillment
of the requirements for

M. S. degree in Chemical Engineering


Major professor

Date 5/17/84



RETURNING MATERIALS:
Place in book drop to
remove this checkout from
your record. FINES will
be charged if book is
returned after the date
stamped below.

--	--	--

SOME KINETIC ASPECTS OF THE GASIFICATION
OF GRAPHITE AND PLATINUM GRAPHIMET

By

Seung I. Choi

A THESIS

Submitted to
Michigan State University
in partial fulfillment of the requirements
for the degree of

MASTER OF SCIENCE

Department of Chemical Engineering

1984

ABSTRACT

SOME KINETIC ASPECTS OF THE GASIFICATION
OF GRAPHITE AND PLATINUM GRAPHIMET

By

Seung I. Choi

The kinetics of the oxidation and steam gasification of graphite and platinum graphimet is presented. The kinetic studies employ temperature programmed desorption/reaction. A scanning transmission electron microscopy of both unreacted and reacted platinum graphimet reveals that the behavior and morphologies are similar to those found by controlled atmosphere electron microscopy.

A correlation using a mathematical model of the temperature programmed desorption/reaction experiments show that platinum increases the density of active sites. This is attributed to the scission of carbon-carbon bonds by platinum. The lowering of the catalyzed oxidation temperature is explained by the scission function of platinum. For platinum, there is some possibility that both electron and oxygen transfer could be operating for the catalyzed reaction. The latter is suggested by a match between Baker's controlled atmosphere electron microscopy studies and a simple mathematical model using the assumptions of viscous oxide layer and surface diffusion.

	Page
List of Figures	iv
Notations	vii
CHAPTER I	
INTRODUCTION	1
LITERATURE REVIEW	
Mechanism of Oxidation	3
Temperature Programmed Desorption	6
OBJECTIVE OF RESEARCH	9
CHAPTER II	
THE TEMPERATURE PROGRAMMED DESORPTION/ REACTION APPROACH OF THE GASIFICATION OF CARBON: EXPERIMENT	
Experimental Method	11
Experimental Results	17
Discussions on Results	37
CHAPTER III	
THE TEMPERATURE PROGRAMMED DESORPTION/ REACTION APPROACH OF THE GASIFICATION OF CARBON: THEORY	
Theory	44
Theoretical TPD Plots	51
Discussion on TPD Plots	59

CHAPTER IV

THE CHANNEL PROPAGATION RATE OF PLATINUM ON A CARBON SURFACE: A MODEL AND STEM STUDIES

Figure 11-1	Background	64
Figure 11-2	STEM of Unreacted and Reacted Platinum Graphimet	67
Figure 11-3	A Mathematical Model of the Catalyst Particle Propagation	89
Figure 11-4	Closures	100

APPENDIX

Figure 11-5A	A. Computer Program and Sample Calculations	101
Figure 11-5B	B. Standarization of G. C. Units	105
Figure 11-5C	C. Solutions to Equations (IV - 1) to (IV - 4)	108

Figure 11-6	LIST OF REFERENCES	112
-------------	--------------------	-----

LIST OF FIGURES

	page
Figure II-1 Schematic diagram of the experimental apparatus	12
Figure II-2 Schematic sketch inside the reactor	13
Figure II-3A Desorption pattern of graphite pre-treatment, $\beta = 30.5^{\circ}\text{C}/3 \text{ min}$	17
Figure II-3B Weight loss pattern of graphite pre-treatment, $\beta = 30.5^{\circ}\text{C}/3 \text{ min}$	18
Figure II-4A Desorption pattern of graphite second heating, $\beta = 30.5^{\circ}\text{C}/3 \text{ min}$	19
Figure II-4B Weight loss pattern of graphite second heating, $\beta = 30.5^{\circ}\text{C}/3 \text{ min}$	20
Figure II-5A Desorption pattern of graphite third heating, $\beta = 29.5^{\circ}\text{C}/3 \text{ min}$	21
Figure II-5B Weight loss pattern of graphite third heating, $\beta = 29.5^{\circ}\text{C}/3 \text{ min}$	22
Figure II-6A Desorption pattern of graphite fourth heating, $\beta = 31^{\circ}\text{C}/3 \text{ min}$	23
Figure II-6B Weight loss pattern of graphite fourth heating, $\beta = 31^{\circ}\text{C}/3 \text{ min}$	24
Figure II-7A Desorption pattern of Pt-graphimet pretreatment, $\beta = 30^{\circ}\text{C}/3 \text{ min}$	25
Figure II-7B Weight loss pattern of Pt-graphimet pretreatment, $\beta = 30^{\circ}\text{C}/3 \text{ min}$	26
Figure II-8A Desorption pattern of Pt-graphimet second heating, $\beta = 27^{\circ}\text{C}/3 \text{ min}$	27
Figure II-8B Weight loss pattern of Pt-graphimet second heating, $\beta = 27^{\circ}\text{C}/3 \text{ min}$	28
Figure II-9A Desorption pattern of Pt-graphimet third heating, $\beta = 31^{\circ}\text{C}/3 \text{ min}$	29

	page
Figure II-9B	Weight loss pattern of Pt-graphimet third heating, $\beta = 31^{\circ}\text{C}/3 \text{ min}$ 30
Figure II-10A	Desorption pattern of graphie H_2O adsorption, $\beta = 29.5^{\circ}\text{C}/3 \text{ min}$ 31
Figure II-10B	Weight loss pattern of graphite H_2O adsorption, $\beta = 29.5^{\circ}\text{C}/3 \text{ min}$ 32
Figure II-11	Desorption pattern of Pt-graphimet H_2O adsorption, $\beta = 28.3^{\circ}\text{C}/3 \text{ min}$ 33
Figure II-12	Steam gasification of graphimet TPD, $\beta = 28^{\circ}\text{C}/3 \text{ min}$ 34
Figure II-13A	Steam gasification of Pt-graphimet TPD, $\beta = 29.4^{\circ}\text{C}/3 \text{ min}$ 35
Figure II-13B	Steam gasification of Pt-graphimet weight loss pattern, $\beta = 29.4^{\circ}\text{C}/3 \text{ min}$... 36
Figure III-1	Schematic sketch of TPD system 45
Figure III-2	Theoretical TPD spectra of carbon/ metal system, $E_C = 260 \text{ KJ/mole}$, $E_m = 230 \text{ KJ/mole}$ 51
Figure III-3	Theoretical TPD spectra of carbon/ metal system, $E_C = 260 \text{ KJ/mole}$, $E_m = 250 \text{ KJ/mole}$ 52
Figure III-4	Theoretical TPD spectra of carbon/ metal system, $E_C = 260 \text{ KJ/mole}$, $E_m = 270 \text{ KJ/mole}$ 53
Figure III-5	Theoretical TPD spectra of carbon/ metal system, $E_C = 260 \text{ KJ/mole}$, $E_m = 280 \text{ KJ/mole}$ 54
Figure III-6	Theoretical TPD spectra of carbon/ metal system, $E_C = 260 \text{ KJ/mole}$, $E_m = 300 \text{ KJ/mole}$ 55
Figure III-7	Theoretical TPD spectra of carbon/ metal system, $E_C = 270 \text{ KJ/mole}$, $E_m = 250 \text{ KJ/mole}$ 56

	page
Figure III-8	Theoretical TPD spectra of carbon/ metal system, $E_C = 270$ KJ/mole, $E_m = 300$ KJ/mole 57
Figure III-9	Theoretical TPD spectra of carbon/ metal system, $E_C = 270$ KJ/mole, $E_m = 350$ KJ/mole 58
Figure IV-1	STEM of unreacted Pt-graphimet 1,000 Å/cm 71
Figure IV-2	STEM of unreacted Pt-graphimet 500 Å/cm 72
Figure IV-3	STEM of unreacted Pt-graphimet 50 Å/cm 73
Figure IV-4	STEM of unreacted Pt-graphimet 20 Å/cm 74
Figure IV-5	X-ray dispersive analysis of Pt-graphimet 75
Figure IV-6	STEM of reacted Pt-graphimet 2,000 Å/cm 76
Figure IV-7	STEM of reacted Pt-graphimet 1,000 Å/cm 77
Figure IV-8	STEM of reacted Pt-graphimet 500 Å/cm 78
Figure IV-9	STEM of reacted Pt-graphimet 100 Å/cm 79
Figure IV-10	Schematic illustration of various channelling activities in Figure (IV-7).. 80
Figure IV-11	Simplified sketch of particle channelling activity - model 88
Figure IV-12	Dependency of channel propagation rate on particle width 98
Figure IV-13	Dependency of channel propatation rate on k 99

NOTATIONS

A_C	Preexponential factor in the carbon phase (sec^{-1})
A_m	Preexponential factor in the metal phase (sec^{-1})
C	Concentration of carbon atoms (moles/ cm^3)
C_{CO}	Concentration of carbon monoxide (moles/ cm^3)
C_O	Concentration of carbon atoms at the carbon-metal interface (moles/ cm^3)
$\frac{C}{C_O}$	C / C_O
\hat{C}	$1 - \frac{C}{C_O}$
D_{cm}	Diffusivity of carbon atoms in the metal matrix (cm^2/sec)
D_{c-mo}	Diffusivity of carbon atoms in the metal oxide layer (cm^2/sec)
D_{cs}	Diffusivity of carbon atoms on the surface of the metal oxide layer (cm^2/sec)
E_C	Activation energy of desorption in the carbon phase (KJ/mole)
E_m	Activation energy of desorption of the metal phase (KJ/mole)
F	Flow rate of carbon monoxide (moles/sec)
h	Plank constant (6.626×10^{-34} J sec)
k	Boltzmann's constant (1.380×10^{-23} J/K)
k_1	First order rate constant (sec^{-1})
\tilde{k}	A thermodynamic constant defined in page 92 (cm^{-1})

K_C	Mass transfer coefficient of carbon atoms	(cm/sec)
k_C	$A_C \exp(-\gamma_C)$	(sec ⁻¹)
k_m	$A_m \exp(-\gamma_m)$	(sec ⁻¹)
L	The metal particle width	(cm)
\dot{n}	Molar flow rate	(moles/sec)
N_C	Flux of carbon atoms	(moles/cm ² sec)
\hat{n}_{CO}	Number of moles of carbon monoxide per unit area	(moles/cm ²)
n_{CO}	Number of moles of carbon monoxide per unit volume	(moles/cm ³)
n	Integers	
Q	Flow rate of carrier gas	(moles/sec)
R	Gas constant	(8.314 J/gmole ^o K)
R_{CO}	Rate of carbon monoxide production	(moles/cm ²)
S	Total effective surface area	(cm ²)
S_C	Effective surface area of carbon phase	(cm ²)
S_m	Effective surface area of metal phase	(cm ²)
SRATIO	S_m / S_C	
T	Temperature of TPD system	(^o K)
T_O	Reference temperature	(298 ^o K)
T_M	Maximum peak temperature of TPD spectra	(^o K)
T_i	Temperature of the inflection point of TPD spectra	(^o K)
u_{CO}^C	n_{CO}^C / n_{CO}^C (1)	
u_{CO}^m	n_{CO}^m / n_{CO}^m (1)	

v	T / T_0	
$\langle v \rangle$	Velocity of channel propagation	(cm/sec)
x, y, z	Cartesian coordinates	
Superscripts		
m	Metal phase	
c	Carbon phase	
s	Surface of metal oxide layer	
Subscripts		
o	Metal-carbon interface	
Greek Symbols		
β	Heating rate	(K/sec)
γ_c	E_c / RT_0	
γ_m	E_m / RT_0	
$\bar{\beta}$	β / T_0	(sec ⁻¹)
ξ	x / L	
ζ	y / L	
ϕ_1	Biot number = $K_c L / D_{cm}$	
ϕ_2^2	$k_1 L^2 / D_{cs}$	
ϕ_3	$D_{cm} L C_o / D_{cs} C_o^s$	
δ	Effective thickness of oxide layer	(cm)
Λ	$C^s(0) / C_o^s$	
ϕ_4	$D_{c-mo} \tilde{k} C_o^s L / D_{cm} C_o \delta$	

SYNOPSIS

Catalytic reactions of carbon and graphite is one of the most intensively investigated topics in the field of catalysis. It is well known that the small, well ordered layers of graphite can act as a catalyst in the oxidation of hydrocarbons, but in the case of the oxidation of hydrocarbons over the year, the reaction is still unexplained.

CHAPTER I

Of course, the most important step in the oxidation of graphite, the adsorption of oxygen on the surface, is the adsorption of oxygen on the surface of catalyst, and the desorption of oxygen from the surface. The most significant work in this field in the literature has been directed toward studies on the adsorption of the catalytic systems and the determination of the kinetic parameters of both the overall reaction and the individual steps mentioned above.

The interaction of oxygen with graphite is of particular importance since it is the catalysis for a number of reactions of hydrocarbons, such as the oxidation of naphthalene and certain hydrocarbons, and an oxidative step is usually employed in the synthesis of various substituted catalysts.

It is the purpose of this review to discuss the details

INTRODUCTION

Catalytic oxidation of carbon and graphite is one of the most interesting and intriguing topics in the field of catalysis. It is well known that extremely small amounts of impurities can have a profound effect on the oxidation rate of graphite, but in spite of considerable efforts made to this topic over the years the precise mechanism of how impurities operate is still unknown.

Of many important steps involved in the gasification of graphite, the breakage of the carbon-carbon bonds by catalyst, the adsorption of reacting gases on the surface of catalyst, and the desorption of products from the surface seem to be the most significant ones, and most works in the literature have been directed toward studies on the characterization of the catalytic surfaces and the determination of the kinetic parameters of both the overall and each of the three steps mentioned above.

The interaction of platinum group metals with graphite is of particular importance since these metals are the catalysts for a number of reactions of commercial interest, e.g., reforming of naphthas and certain hydrogenations, and an oxidation steps is usually employed to reactivate a carbon contaminated catalyst.

It is the purpose of this research to examine the details

of the catalytic effect of platinum on the gasification of carbon with the use of Temperature Programmed Desorption and Scanning Transmission Electron Microscopy and to pursue an understanding of the catalytic mechanism, especially of the oxidation of carbon.

It is well known that the mechanism of carbon oxidation is very complex. The mechanism of carbon oxidation has been used to explain the catalytic activity of platinum in carbon oxidation. It is generally accepted that the active sites of the catalyst are the platinum atoms on the surface of the carbon. With the development of the oxygen-adsorption on the side surface of platinum, the mechanism of carbon oxidation is generally understood. The oxygen transfer mechanism of the active catalyst is considered as an oxygen carrier which perhaps undergoes a periodic process of oxidation-reduction cycles as a carbon surface during the progress of reaction. An intermediate compound such as a metal oxide is formed, and is reduced upon contact with the carbon substrate at the metal-carbon interface. Recently, the catalytic mechanism of carbon oxidation by H_2 , H_2O and CO_2 by Hatakeyama and Washida (1981) stress that the ability of the platinum to directly break carbon-carbon bonds within the gasification of adsorbed gas on the catalyst surface and the catalyst may also be capable of dissociatively adsorbing and dissociating with respect to the adsorbed carbon on the catalyst surface.

LITERATURE REVIEW

A. Mechanism of Oxidation of Carbon

While there has been a surge in the number of experiments on metal-catalyzed oxidation of carbon, only a few have attempted to offer the mechanism of the oxidation process. This adversity is mainly attributed to the paucity of information regarding the mechanism. There are two mechanisms that have been used to explain the activity of metal catalysts in carbon oxidation. In the electron transfer mechanism (11, 12), the catalyst serves to either donate or accept electrons to or from the carbon. With the weakening of the carbon-carbon bond on the edge planes of carbon, the dissociative chemisorption of oxygen is greatly enhanced. In oxygen transfer mechanism (13), the active catalyst is considered as an oxygen carrier which perhaps undergoes a periodic number of oxidation-reduction cycles on a carbon surface during the progress of reactions. An intermediate compound such as a metal oxide is formed, and is reduced upon contact with the carbon substrate at the metal-carbon interface. Recently, the catalyzed carbon-carbon bond breakage mechanism has been proposed for carbon gasification by H_2 , H_2O and CO_2 by Holstein and Boudart (14, 15). They stress that the ability of the catalyst to directly break carbon-carbon bonds without the participation of adsorbed gas on the catalyst surface, and the catalyst must also be capable of dissociatively adsorbing gas molecules which react with the adsorbed carbon on the catalyst surface.

It now appears as a consensus that a whole set of physico-chemical factors govern the rates of metal/metal oxide catalyzed oxidation of carbon on a graphite basal surface.

Two of these factors are effective catalyst particle size and the oxidation state of the metal. The particle size of the metals and metal oxides often dictates the magnitude of the rate of carbon oxidation, and sometimes it is generally adopted as a characterization of metal/metal oxide catalytic oxidation of carbon. As in most of Baker's and his co-workers studies, the channel propagation rate of a single catalyst particle is always adopted as the basis for estimating the magnitude of the catalytic attack rate of graphite surfaces. The channel propagation rate, as observed by Controlled Atmosphere Electron Microscope (CAEM), is inversely proportional to the particle size, expressed in terms of particle width, for the oxidation process (16, 17, 18, 19, 20). On the contrary, for the metal catalyzed hydrogenation of graphite surfaces, the channel propagation rate has a quadratic dependency (17). Baker and Sherwood (17) therefore conclude that there exists a fundamental difference in the mechanisms of carbon oxidation and hydrogenation. Keep et al. (21) have proposed two mechanisms for catalytic reduction of graphite. In the first mechanism, the metal catalyst acts as a dissociation center for hydrogen, producing atoms which diffuse across the metal/carbon interface and react with the carbon to produce methane. In the second mechanism, carbon atoms at the interface dissolve into the metal and diffuse to the

exposed particle surfaces to react with hydrogen. Baker and Sherwood (17) support the first mechanism as a more rational model from their investigations involving silica inclusions in small nickel particles, and they further conclude that the metal catalyzed oxidation of graphite is also diffusion-controlled.

Holstein and Boudart (14), in their study of the platinum catalyzed hydrogenation of graphite, argued that hydrogen spillover, and thus, surface diffusion was not a viable mechanism and could not be a limiting process. They hypothesized that the cleavage of carbon-carbon bonds by the metal could be the limiting process.

Another important aspect of the metal-catalyzed oxidation of carbon is the chemical state of the metal. The oxidation state of the catalyst has been found to have a significant effect on the rate of carbon oxidation. For instance, iron is very active in the CO_2 oxidation of carbon, Wustite (FeO) is less active and magnetite (Fe_3O_4) is totally inactive (13). In the oxidation of graphite by Ni, Baker and Sherwood (17) speculated that a thin oxide layer of NiO was responsible for the passivism of the nickel catalyst towards C-O_2 reaction. For such metals as Ag, Pb, and Pt, the rate of the catalyzed oxidation of carbon is not drastically influenced by their oxidation states. The observation of the dynamics of metal oxides formation during the course of carbon oxidation is yet beyond in situ analysis, and the speculation of metal oxide formation is usually done by inference.

B. Temperature Programmed Desorption

Various techniques are used to study the gas-solid surface interactions, such as flash-filament desorption, selective poisoning, field electron and ion microscopy, etc. Temperature Programmed Desorption (TPD) method is in principle similar to flash-filament desorption, but TPD method can be applied to any type of solid catalysts and situations where the experimental conditions need be closer to those in actual practice. A detailed description of TPD and its applications is given by Cvetanovic and Amenomiya (1, 2).

The simplest model by Cvetanovic and Amenomiya (1) assumes linear heating schedule, first-order desorption, homogeneous surface, negligible diffusional effects and negligible readsorption, and gives the following equation relating the maximum peak temperature to the apparent activation energy of desorption.

$$2 \ln(T_M) - \ln(\beta) = E_d/RT_M + \ln(E_d/AR) \dots \dots \dots (I-1)$$

When readsorption occurs freely during desorption, the peaks are much broader, and readsorption can be minimized by increasing the carrier-gas flow rate. Unlike the theoretical arguments by Cvetanovic and Amenomiya, Gorte (3) argues that readsorption in porous catalysts cannot be eliminated even for desorption into a vacuum, and readsorption can easily change the desorption temperature by several hundred K. Hertz et al (4) studied desorption of carbon monoxide into a vacuum for a 1.0 wt % platinum on porous γ - Al_2O_3 , and compared their results with those by Fogar and Anderson (5) who did the same

experiment using a carrier gas instead of vacuum. They found that the peak temperature in the case of vacuum desorption was about 80°K higher than that in the case of desorption into a carrier gas, and in both cases adsorption competed with desorption to the extent that adsorption equilibrium was closely approached at each point in a porous sample.

In the case of desorption from heterogeneous surfaces, theoretical analyses of TPD model become more elaborate. Cvetanovic and Amenomiya (2) used the Arrhenius equation to define the dependence of rate constant on temperature, and assumed that the activation energy of desorption was a linear function of surface coverage. They found from calculations that TPD spectra had a broad energy spread on a heterogeneous surface, and as a potential example showed the desorption spectrum of carbon monoxide from a sample of platinum deposited on cabosil. Taylor and Weinburg (6) developed a model for analyzing TPD spectra to determine the coverage dependence of the preexponential factor and the desorption energy in the Arrhenius equation for a one-step desorption process. They showed that both rate parameters had a strong coverage dependence in the case of carbon monoxide desorption from Ir (110), and concluded that among several limitations their model was not appropriate for systems involving desorption from several distinct sites. Barton and Harrison (7) studied desorption of surface oxides after chemisorption of oxygen on graphite, and found that desorption of the oxides formed during chemisorption was mainly in the form of carbon monoxide and the surface was reasonably uniform with

an activation energy of desorption of 276 KJ/mole. They further concluded that the activation energies of oxidation and those of desorption of oxide were so close that the oxidation of graphite proceeded in two steps, formation of surface oxide and desorption of this oxide, and the desorption could be rate controlling. They also found that the amount of oxide desorbed after chemisorption was substantially less than that found during the initial degassing, corresponding to oxide areas of $9.0 \text{ m}^2/\text{g}$ and $6.4 \text{ m}^2/\text{g}$ respectively. Although they did not carry out the third heating of the same sample after the second chemisorption of oxygen to make this trend clearer, they still concluded that the heat treatment during the initial degassing rendered part of the graphite surface incapable of reforming oxide. Other workers have explained this. Harker et al. (8) interpreted the reduced reactivity in terms of the annealing of basal plane dislocations, while Mrozowski and Andrews (9) interpreted their results by assuming that free valencies caused by the grinding process were capable of bonding with adjacent free valencies leaving a chemically inactive surface.

When desorbing species has an appreciable surface reaction rate during desorption, Gorte and Schmidt (10) shows that reaction parameters can only be obtained from TPD experiments when reaction occurs in the same temperature range as desorption, and in the limit of low coverage one rate parameter kinetics may be applicable in most systems with heating rate being the most useful variable in extracting reaction parameters. They also conclude that the desorption peaks shift to higher temper-

atures and are narrower than would be predicted by their desorption parameters alone.

OBJECTIVE OF THE RESEARCH

This work reexamine the platinum catalyzed oxidation of carbon, with emphasis on understanding the underlying kinetics and catalytic function of platinum. We aim to investigate the following:

- (1) platinum as an agent for carbon-carbon bond scission
- (2) oxygen and electron transfer mechanism
- (3) existence of viscous layer of metal oxide
- (4) the feasibility of employing temperature programmed desorption/reaction in studying the kinetics of catalyzed and uncatalyzed oxidation of carbon
- (5) assess the catalytic behavior of platinum graphimetric using scanning transmission electron microscopy.

CHAPTER II

THE TEMPERATURE PROGRAMMED DESORPTION/REACTION APPROACH OF THE GASIFICATION OF CARBON:

EXPERIMENT

The furnace used in this experiment was a 1.5 inch I.D. tube furnace with a length of 12 inches. It was suspended from a 2.5 inch diameter steel shaft 14 feet long and was supported by two 1000 watt Lindberg tubular heaters. The temperature of the furnace was varied by a 1000 watt resistor of the proportional integral type. A thermocouple was placed in this quartz tube and was used to monitor the sample zone for the temperature programmed reaction. The voltage readings were converted by a millivoltmeter, which converted into degrees Fahrenheit using a conversion table provided by Omega Corporation. (The details of the furnace are given in Table I.)

A. Catalyst

The catalyst used throughout the experiment was a fine platinum graphite which is known as "Platinum Graphite" by the Omega Corporation. Although platinum is known to be a good catalyst

EXPERIMENTAL METHOD

This chapter discusses the temperature programmed desorption/reaction experiments for the oxidation of graphite and platinum graphimet.

A. Design of the Apparatus

A schematic diagram of the experimental set-up is given in Figure (II-1).

The quartz reactor tube was 30 inches long and 1.5 inch I.D. The sample of catalyst powder (typically 50 mg) was suspended from a Cahn 1000 microbalance with a quartz fiber (4 feet long and 500 microns in diameter) into the center of the quartz tube reactor which was surrounded by 1400 watts Lindberg tubular turnace of 2 inches I.D. The temperature of the furnace was varied by Lindberg Furnace Controller of the proportional integral type. Chromel-Alumel thermocouple enclosed in a thin quartz tube was placed right next to the quartz sample pan for the temperature measurements of the sample. The voltage readings were monitored by a potentiometer, and converted into degrees Fahrenheit using a conversion table provided by Omega Corporation. (For details of the reactor, see Figure (II-2).

B. Catalyst

The catalyst used throughout the experiment was a 1 wt. % platinum graphimet which is commercially produced by the Ventron Corporation. Although graphite cannot be directly intercalated

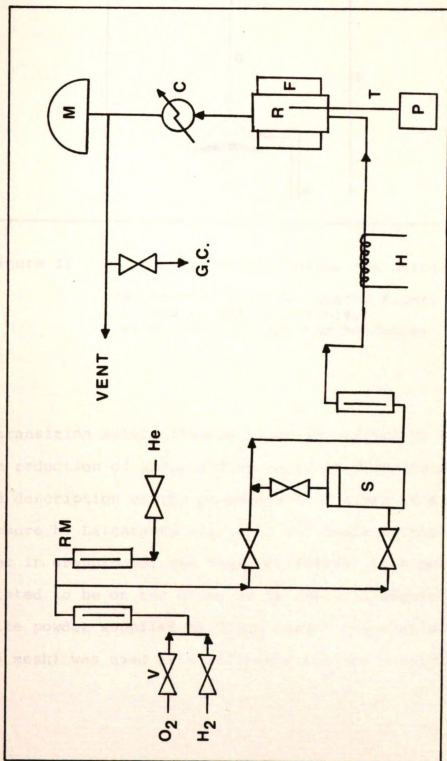


Figure II-1 Schematic Diagram of Experimental Apparatus
 (V: needle valve, RM: rotameters, S: H_2O saturator, R: reactor, F: furnace, P: potentiometer, T: thermocouple, C: cooler, M: microbalance, H: heating tape)

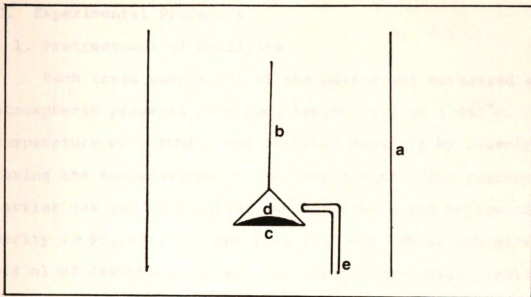


Figure II-2 Schematic Sketch Inside the Reactor

(a: reactor wall, b: quartz fiber,
 c: quartz pan, d: sample,
 e: quartz tube for thermocouple)

with transition metal, intercalation is claimed to be possible by the reduction of intercalated salts of these metals. A detailed description of the preparation is given in a U.S. patent disclosure by Lalancette (29). On the basis of the total metal content in graphimets, the distance between each metal atom is calculated to be on the order of 5\AA (30). A highly purified graphite powder supplied by Ultra Carbon Corporation (Type UCP-2, 325 mesh) was used as a reference for the catalytic study.

C. Experimental Procedure

1. Pretreatment of Catalysts

Each fresh sample out of the bottle was outgassed at one atmospheric pressure from room temperature to $1,000^{\circ}\text{C}$. Linear temperature programming was obtained manually by closely monitoring the temperatures of the sample within the reactor. The carrier gas used throughout the experiment was helium of high purity ($> 99.99\%$), and the flow rate was set at 200 ml/min. 0.4 ml of desorbing gas was collected into a high precision syringe from the sample collecting flask every three minute and injected into the Varian 3700 Gas Chromatograph equipped with a thermal conductivity detector for gas analysis. Controlled volumes of reference gases of known concentrations were also injected into the gas chromatograph for standardization and quantification of sample gases from experiments. The standardization procedure is given in Appendix.

The signals of gas chromatograph of products were converted into concentrations according to the standardization, and the concentrations in gram moles were plotted as a function of temperatures in Celsius.

2. Controlled Adsorption

After pretreatment in helium up to $1,000^{\circ}\text{C}$, the sample was cooled down to room temperature at atmospheric pressure with helium gas continuously flowing through the system during the entire cooling period. During controlled oxygen chemisorption, surface oxides were formed at 25°C by exposing the pretreated

sample to an oxygen pressure of 20 psig for 30 minutes.

H₂O adsorption was performed at 300°C by flowing helium gas which was saturated with H₂O at 25°C in the H₂O saturator into the system for 30 minutes.

3. Temperature Programmed Desorption

After the controlled adsorption, the sample was outgassed in helium at a flow rate greater than 500 ml/min for 20 minutes at the adsorption temperature to remove any traces of oxygen in the system. The methods of linear temperature programming and sample collection were the same as in the pretreatment. Concentrations of desorption products, CO, CO₂, CH₄, and H₂ were expressed in terms of gram moles and plotted as a function of temperature. Since the sample size was 0.4 ml, and the carrier gas flow rate was 200 ml/min, the concentrations in gram moles can be converted to the rate of total production in gram moles/min by multiplying them by a factor of 500. After the outgassing up to 1000°C, the sample was again cooled down to room temperature in the presence of flowing helium, and the same procedures were repeated for controlled adsorption and linear temperature programmed heating to obtain second and third concentration versus temperature plots. After the third heating, the sample was cooled to room temperature, and collected for scanning transmission electron microscopic analysis.

4. Gasification and Oxidation

Steam gasification was performed with a fresh sample.

Helium gas saturated with H_2O at room temperature was continuously fed into the system at 200 ml/min, and the temperature was raised from room temperature up to $1,000^\circ C$ in an approximately linear fashion.

Oxidation was performed isothermally at temperatures above $500^\circ C$ with helium at a rate of 200 ml/min, and the gas sample were collected for analysis after a steady weight decrease was observed on the recorder for at least 10 minutes.

EXPERIMENTAL RESULTS



Scale vs. Time
x 10⁻⁵

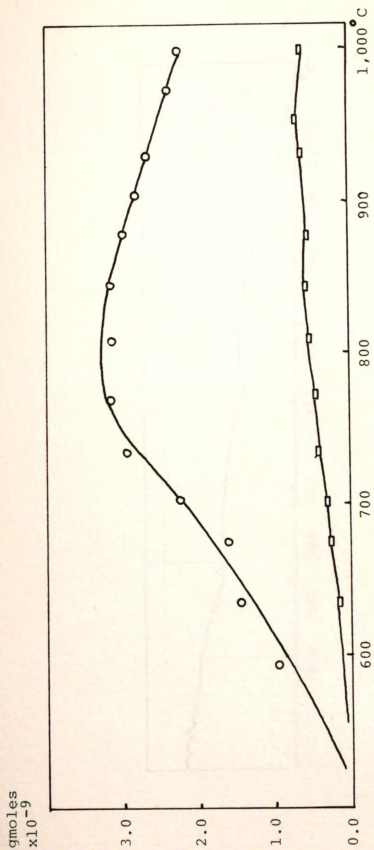


Figure II-3A Desorption Pattern of Graphite

CO (○), CO₂ (□)Pretreatment, $\beta = 30.5^\circ\text{C}/3 \text{ min}$

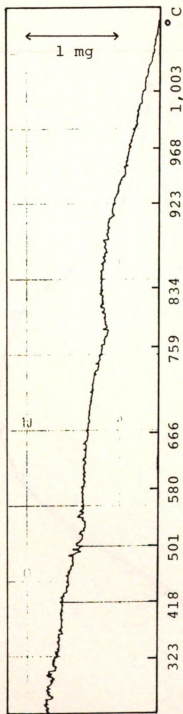


Figure II-3B Weight Loss Pattern of Graphite

Pretreatment, $\beta = 30.5^{\circ}\text{C}/3 \text{ min}$

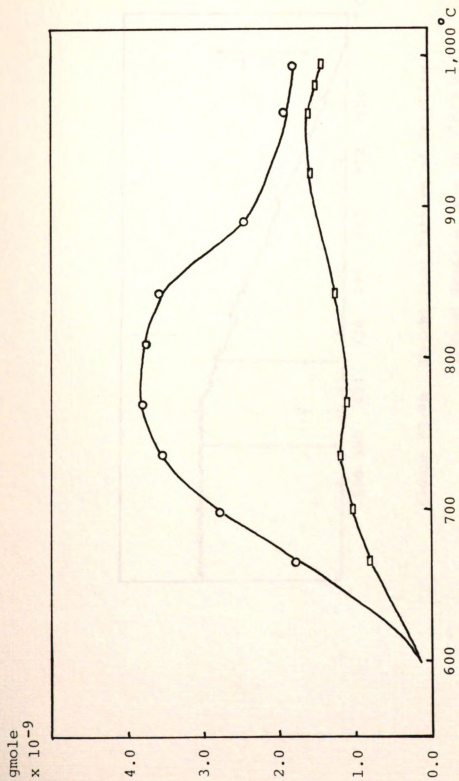


Figure II-4A Desorption Pattern of Graphite
CO (○), CO₂ (□)
Second Heating, $\beta = 30.5^{\circ}\text{C}/3 \text{ min}$
30 min O₂ Exposure at 25°C

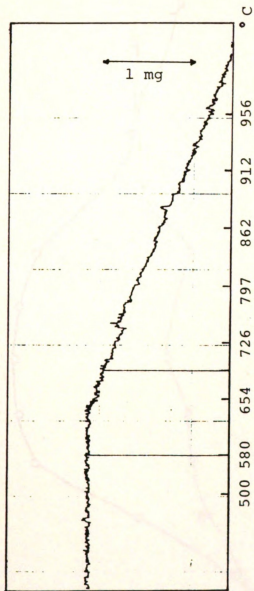


Figure II-4B Weight Loss Pattern of Graphite
Second Heating, $\beta = 30.5^{\circ}\text{C}/3 \text{ min}$
30 min O_2 exposure at 25°C

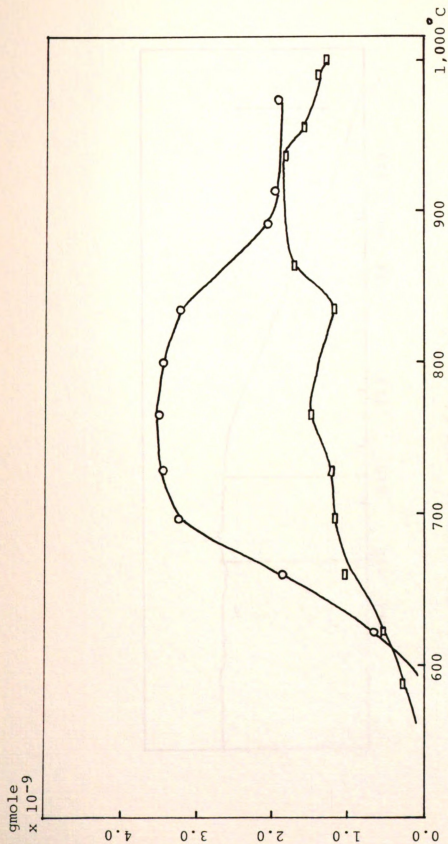


Figure II-5A Desorption Pattern of Graphite

CO (○), CO₂ (□)Third Heating, $\beta = 29.5^\circ\text{C}/3\text{ min}$
30 min O₂ exposure at 25°C

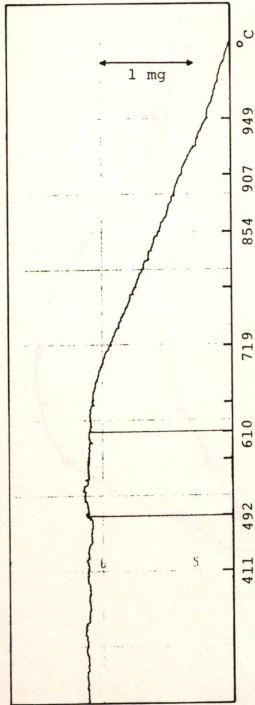


Figure II-5B Weight Loss Pattern of Graphite

Third Heating, $\beta = 29.5^{\circ}\text{C}/3 \text{ min}$
30 min O_2 exposure at 25°C

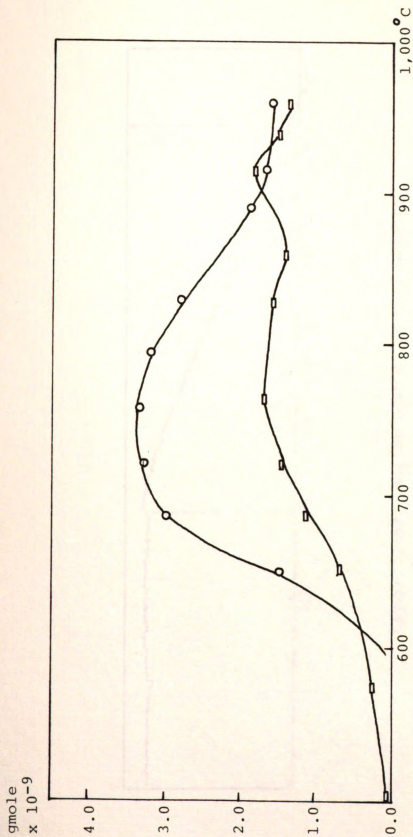


Figure II-6A Desorption Pattern of Graphite

CO (○), CO₂ (□)Fourth Heating, $\beta = 31^\circ\text{C}/3\text{ min}$
30 min O₂ exposure at 25°C

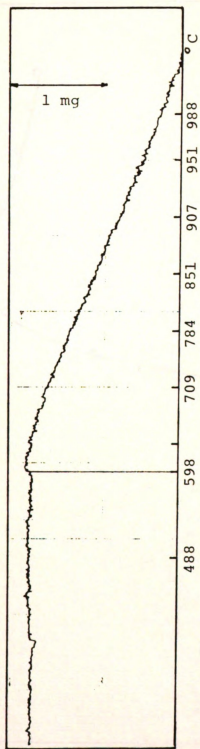


Figure II-6B Weight Loss Pattern of Graphite
Fourth Heating, $\beta = 31^\circ\text{C}/3\text{ min}$
30 min O_2 exposure at 25°C

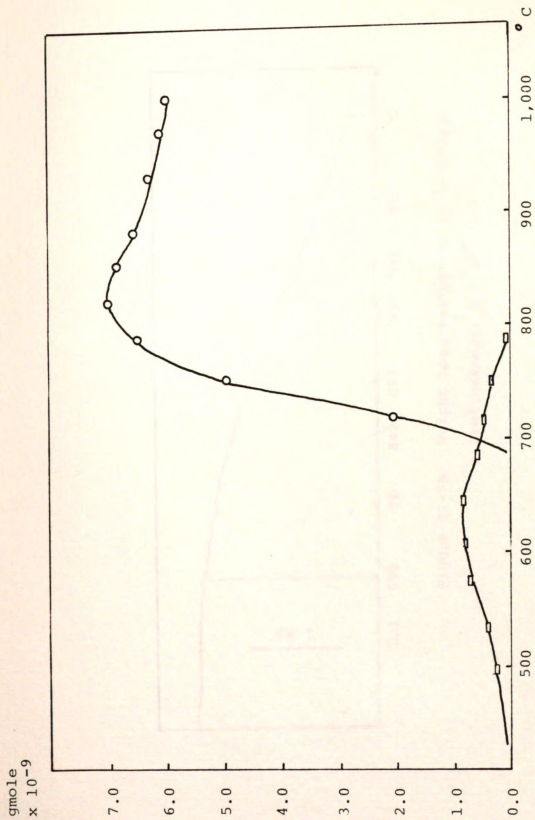


Figure II-7A Desorption Pattern of Pt-Graphimetric

CO (\circ), CO₂ (\square)Pretreatment, $\beta = 30^{\circ}\text{C}/3\text{ min}$

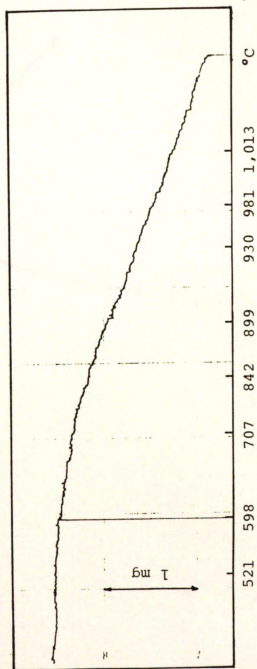


Figure II-7B Weight Loss Pattern of Pt-Graphimetric
Pretreatment, $\beta = 30^{\circ}\text{C}/3 \text{ min}$

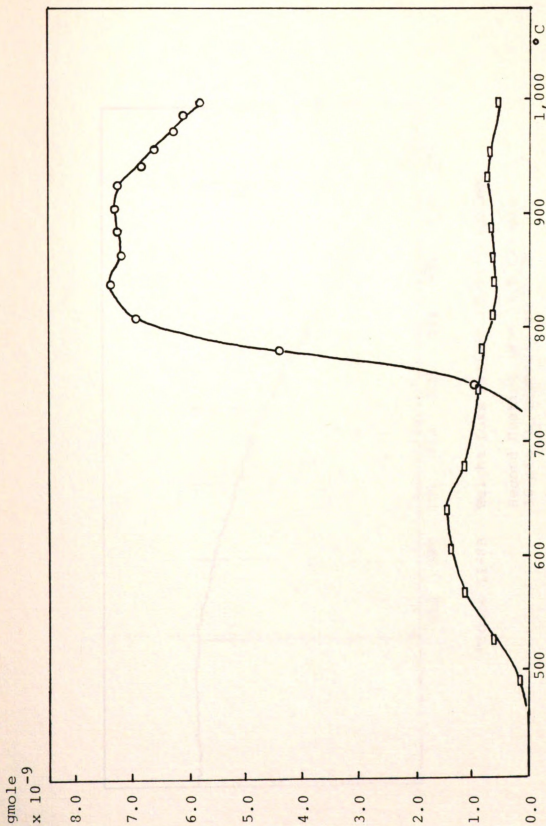


Figure II-8A Desorption Pattern of Pt-Graphimetric

CO (\circ), CO₂ (\square), Second Heating, $\beta = 27.0^{\circ}\text{C}/3 \text{ min}$, 30 min O₂ exposure at 25 $^{\circ}\text{C}$

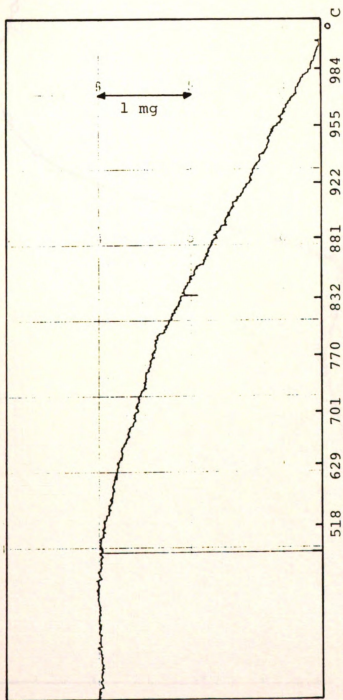


Figure II-8B Weight Loss Pattern of Pt-Graphimetric

Second Heating, $\beta = 27.0^{\circ}\text{C}/3 \text{ min}$
30 min O_2 exposure at 25°C

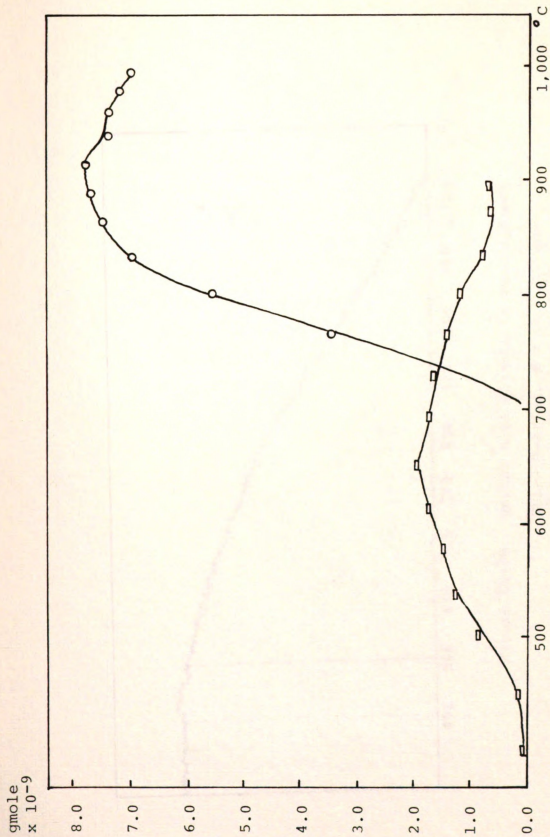


Figure II-9A Desorption Pattern of Pt-Graphimetric
 CO (O), CO₂ (□), Third Heating,
 $\beta = 31.0^\circ\text{C}/3 \text{ min}$, 30 min O₂ exposure at 25°C

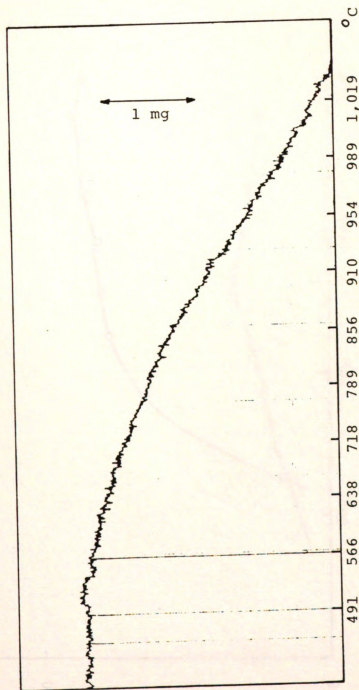


Figure II-9B Weight Loss Pattern of Pt-Graphimetric

Third Heating, $\beta = 31.0^{\circ}\text{C}/3 \text{ min}$
30 min O_2 exposure at 25°C

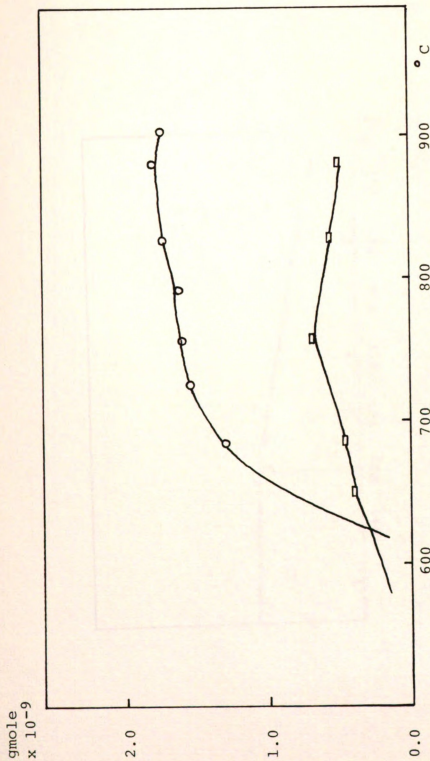


Figure II-10A Desorption Pattern of Graphite

CO (○), CO₂ (□)30 min H₂O exposure at 300°C $\beta = 29.5^{\circ}\text{C}/3 \text{ min}$

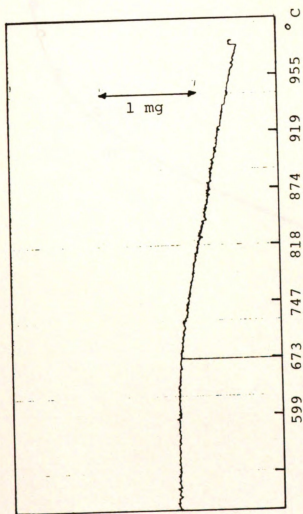


Figure II-10B Weight Loss Pattern of Graphite
30 min H₂O exposure at 300°C
 $\beta = 29.5^\circ\text{C}/3 \text{ min}$

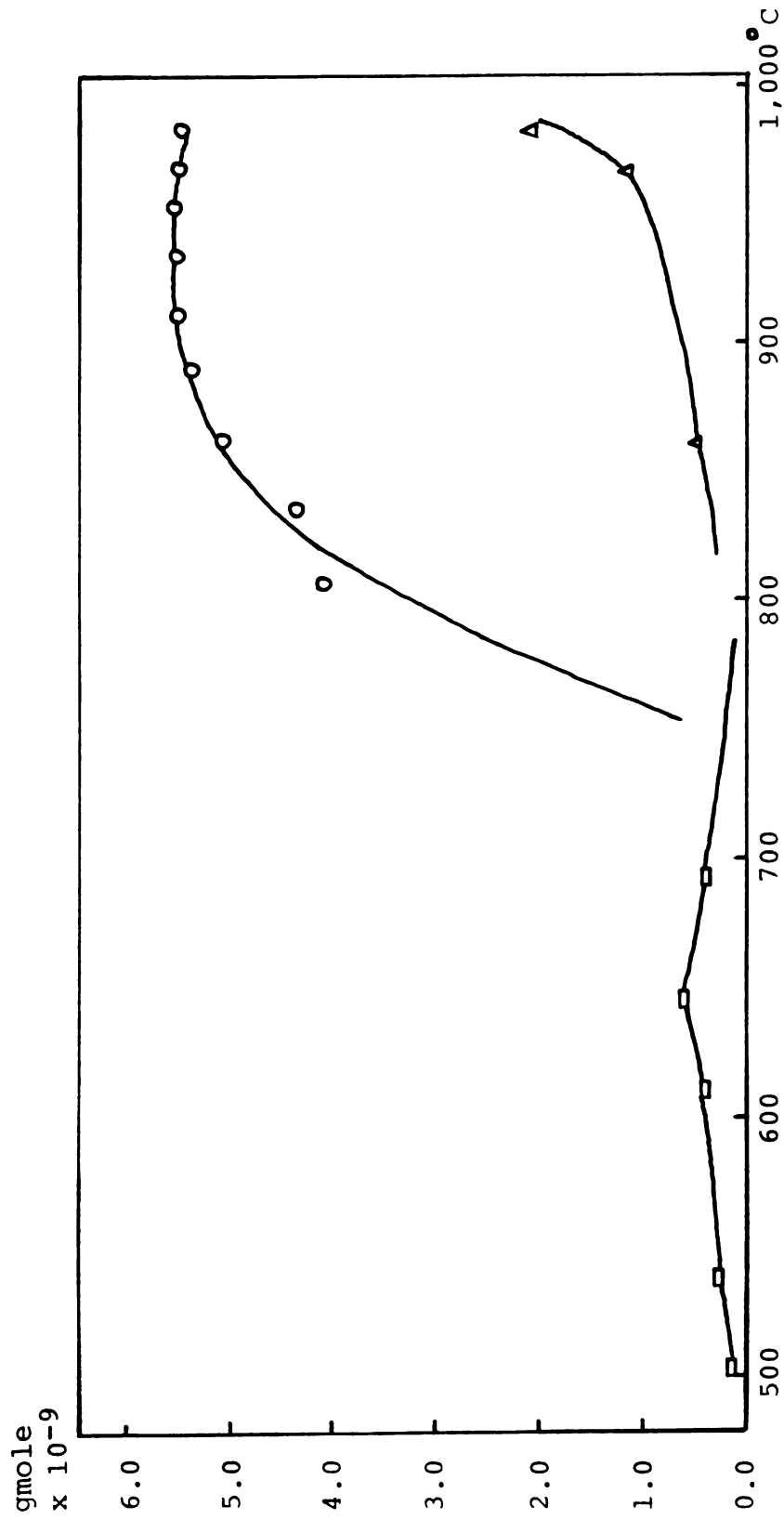


Figure II-11 Desorption Pattern of Pt-Graphimetric

CO (\circ), CO_2 (\square), H_2 (\triangle)
 30 min H_2O exposure at 300°C
 $\beta = 28.3^\circ\text{C}/3 \text{ min}$

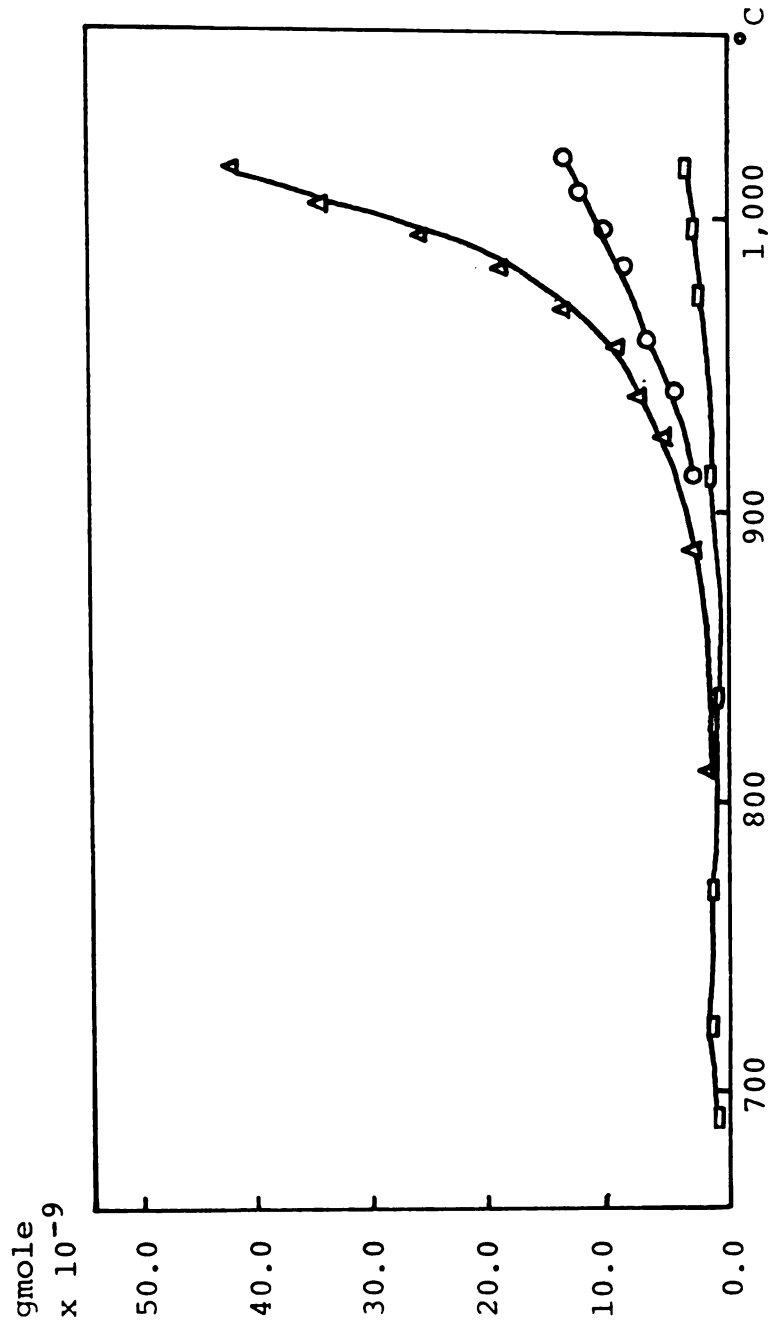


Figure II-12 Steam Gasification of Graphite

CO (○), CO₂ (□), H₂ (△)

$\beta = 28^{\circ}\text{C}/3 \text{ min}$

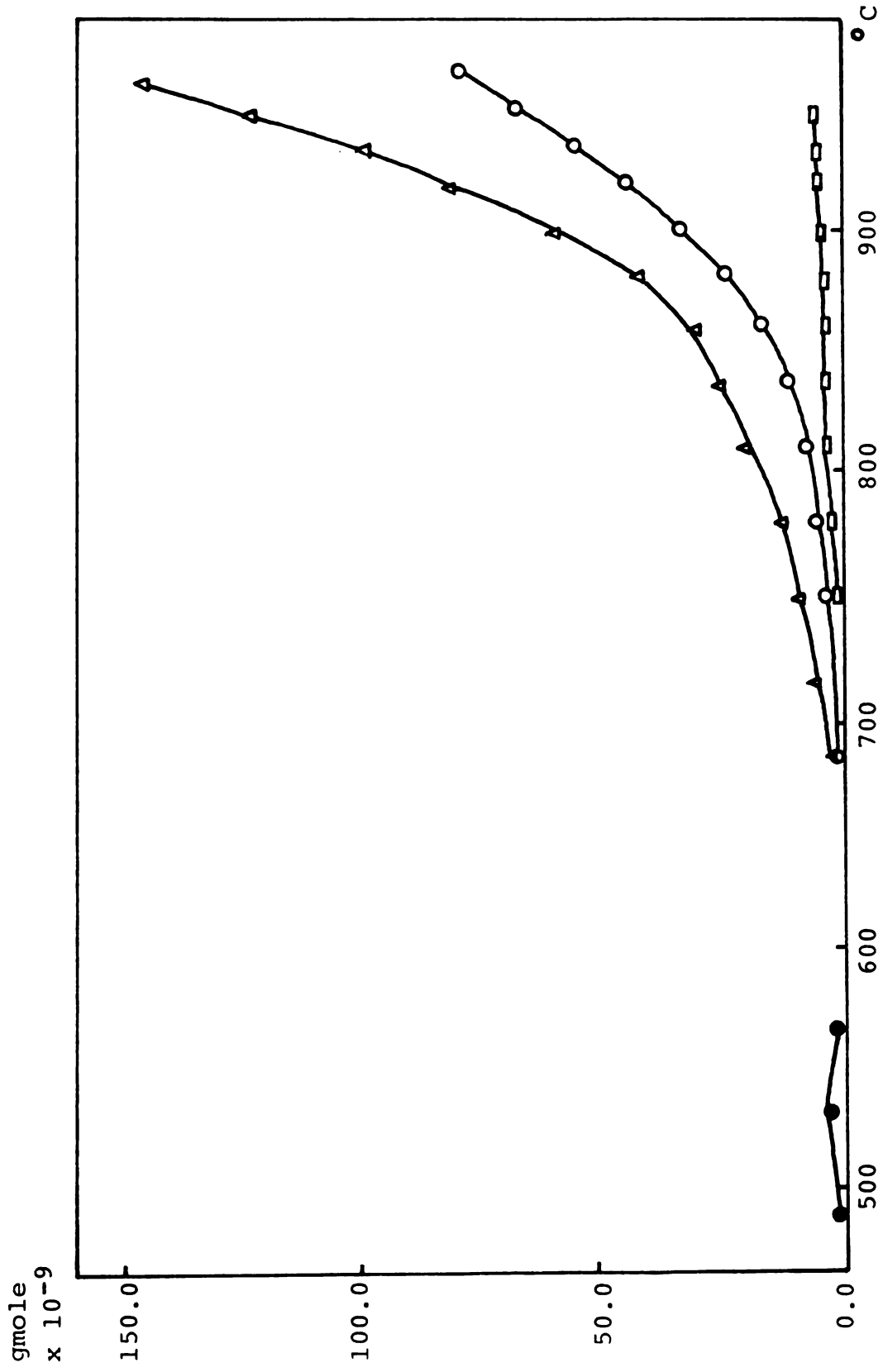


Figure II-13A Steam Gasification of Pt-Graphimnet
 CO (○), CO₂ (□), H₂ (△), CH₄ (●)
 $\beta = 29.4^\circ\text{C}/3 \text{ min}$

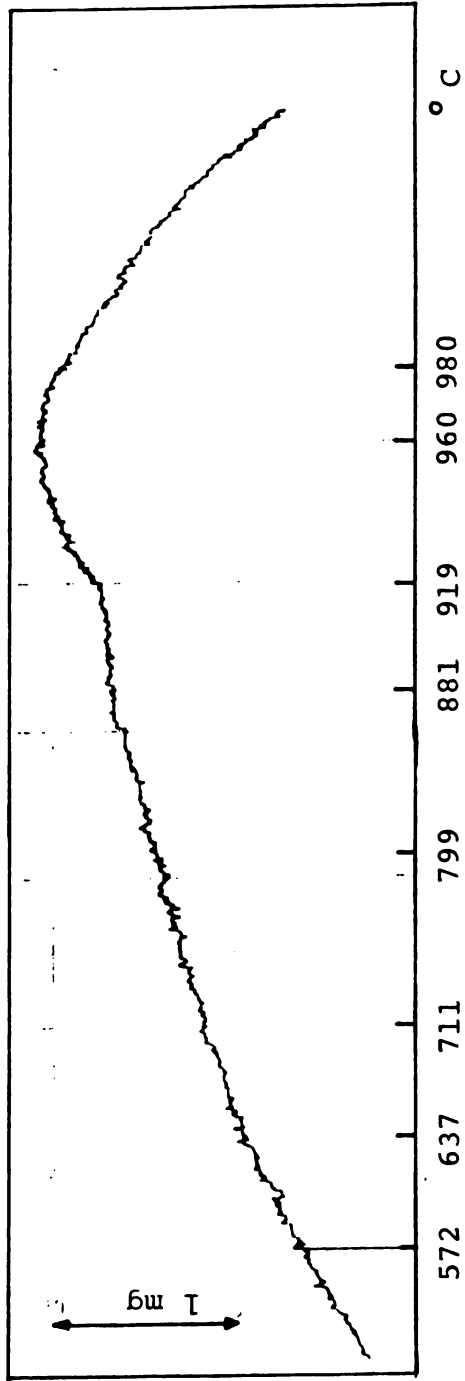


Figure II-13B Weight Loss Pattern of Steam Gasification
of Pt-Graphimmet
 $\beta = 29.4^\circ \text{C}/3 \text{ min}$

DISCUSSIONS ON EXPERIMENTAL RESULTS

A. Pretreatment

Figure (II-3A) shows the desorption patterns of CO and CO₂ from pure graphite during initial outgassing up to 1,000°C. The TPD spectrum of CO is rather broad with a maximum at 800°C, and that of CO₂ is relatively flat with no distinct peak. The rate of CO evolution at 800°C is 1.65×10^{-6} mole/min, about six times greater than that of CO₂ evolution. No distinct spectrum pattern and considerably small rate of production seems to justify the assumption of negligible CO₂ production. As expected, the CO spectrum has only one maximum, and even at this low product concentration a moderate readsorption, or product retardation, in the sample can be seen to occur, since the peak decays rather slowly after the maximum. Due to some disturbances such as noises and shocks, Figure (II-3B) does not show any significant trend of weight loss at each temperature except an overall weight loss of 1.1 mg up to 1,000°C. Both Figure (II-3A) and (II-3B), however, shows that a significant desorption of surface oxides begins to take place at about 600°C.

In Figure (II-7A), the desorption pattern of CO₂ from graphimet is well developed with a maximum at about 625°C, while the CO spectrum has one maximum at about 825°C with a rate of 3.55×10^{-6} mole/min, about eight times greater than that of CO₂ from graphimet and about 2.2 times greater than that of CO from pure graphite. The evolution of CO₂ takes place

below 500°C, compared with 600°C for graphite.

B. Temperature Programmed Desorption

1. Graphite

Figure (II-4A) shows a very broad but symmetric peak of CO during the second heating. The broadness of the peak and the slow decay at higher temperature indeed suggest that the desorption was strongly retarded by CO, as it is by H₂ reported by Blakely and Overholser (22). Foger and Anderson (5) attributed the breadth of the desorption band with smaller secondary peaks over the span of about 400°K to the presence in the sample of a distribution of adsorption sites with different CO binding energies. Their explanation is reasonable in view of the complex surface structure of supported metal particles and the possible influence of the oxide support on small metal particles. However, for pure graphite sample and graphimet used in this experiment, neither such an influence of support material on metal nor the broad spread of different binding energies are expected to exist, and this can be easily seen just by noting a unique and symmetric peak for pure graphite.

It can also be observed from Figures (II-5A) and (II-6A) that the peak temperatures decreased upon successive heating. For the second heating, the actual peak temperature appeared to occur between 775°C and 810°C, and thus, the apparent peak temperature is estimated to be 780°C. For apparent peak temper-

atures for the third and fourth heating were found to be 760°C and 750°C , respectively.

One possible explanation for this observation is that some amount of residual oxygen atoms were left within the sample even after the outgassing up to $1,000^{\circ}\text{C}$ probably because of the atmospheric pressure, and the desorption of oxides would be more diffusion controlled during the next outgassing which could result in the lowering of the apparent activation energy or the apparent peak temperature. In all cases, a significant weight decrease was not observed until the temperature reached about 640°C , 40°C higher than that in the pretreatment, and this small increase seems to be due to the fact that the controlled chemisorption for 30 minutes formed relatively stable oxides only on the graphite surface, which can be verified by the sharper and better defined peaks. And as shown by Hertz et al. (4), these peak temperatures are expected to be a little higher if the experiment were run under vacuum. Since under vacuum the readsorption phenomenon would be less significant, resulting in a higher peak temperature at a greater peak intensity. Assuming a lowering of about 40°C of the peak temperature due to readsorption, the use of Equation (I-1) gave the activation energy of desorption of 300 KJ/mole with a typical experimental value of 760°C for T_M . The preexponential factor, A , was approximated by $KT/h = 2.13 \times 10^{13} \text{ sec}^{-1}$ for the calculation (23).

The activation energy of desorption of CO found by other

experimental methods ranges from 259 to 293 KJ/mole (7, 24, 25), and the close agreement of our calculated value seems to indicate that the assumptions claimed by Equation (I-1) were reasonably well met in our experiment.

2. Graphimet

As in the case of graphite, the total weight loss was constant at 2.4 mg, about twice as large as that in the pretreatment, and at about 510°C, a significant weight decrease began to occur, compared with 600°C in the pretreatment of graphimet and about 640°C in the TPD of graphite shown in Figures (II-8B) and (II-9B). This lowering of temperature, about 130°C, over the graphite suggests the definite catalytic effect of platinum in the oxidation of graphite. Another interesting observation is that the peaks seemed to be resolved into two secondary peaks, and the peak temperatures increased as the heating was repeated. It is not very clear at this point whether the resolution indicates two distinct peaks or just one broad peak with some flat region in it, although a non-uniform energy distribution on the surface appeared to cause the broadness of the peak. In either case, however, the center of the peak shifted to higher temperatures from one run to the next, and this observation is exactly the opposite of that made in the runs with graphite. Although it seems to be not plausible to use Equation (I-1) for the calculation of the activation energy of desorption because of the clearly stronger heterogeneity of the surface of graphimet than that of graphite, the

activation energy of desorption of graphimet is expected to be a little higher than that of graphite, since the apparent peak temperature of graphimet is higher by more than 100°C. The possibility of an increase in activation energy due to catalysis has been reported to hold for carbon gasification by oxygen (26), but whether the increase observed in our case was due to the actual increase in the activation energy of desorption or not is uncertain.

However, unlike in the case of graphite where surface oxides were expected to be formed upon the adsorption of oxygen atoms, the oxygen atoms adsorbed on the metal surface have to combine with carbon atoms at elevated temperatures before the desorption of products takes place. Winicur (27) found that by using a Low-Energy Molecular-Beam-Scattering (LEMS) technique, the desorption of CO from a Pt (111) crystal was adequately represented by a first order Arrhenius form with an activation energy of desorption of 130.2 KJ/mole and a preexponential factor of $2.7 \times 10^{13} \text{ sec}^{-1}$. This low activation energy of desorption clearly suggests a strong influence of the carbon-carbon bond breakage by the metal and probably by the diffusion limitations imposed upon the overall TPD results for graphimet. Otto and Shelef (28) explained the increased activation energies of graphimets with burn-off % in terms of pore diffusion. They concluded that the lower activation energies, observed for fresh samples, were caused primarily by diffusion barriers and as the pore structure opened up during gasification, pore

diffusion became less important resulting in the increase in activation energies. Their explanation was further confirmed by the X-ray diffraction study, and our experimental observation of the increase in the peak temperature with repeated heatings appears to be well explained by their argument. As a consequence, it seems to be reasonable to relate the peak temperature to the apparent activation energy even in the graphimet sample as well as in the graphite and assume that the apparent activation energy of graphimet is at least as high as that of graphite. Therefore, the increased overall rate of CO evolution of graphimet over that of graphite can be attributed to the increase in the preexponential factor in the Arrhenius rate expression, and this conclusion strongly suggest that the cleavage of the carbon-carbon bonds may be the most significant step in the metal catalyzed oxidation of carbon, if not the rate-determining step.

The increased rate of the second and third run, as observed by the doubled weight loss compared with that in the pretreatment, would be due to the opening-up of the pore structure resulting in greater oxygen chemisorption on the surface of metal particles. However, in spite of the residual oxygen atoms in the sample after one run, the observed overall weight loss of the third run was virtually the same as that of the second run. This seems to have resulted from the decrease in active metal surface area due to the agglomeration, and Otto and Shelef (28) found from their X-ray diffraction studies that

after an eight-hour heat treatment at 900°C , metal particles became noticeable in the graphimets, and the diffraction pattern characteristic of the graphimet was gone. All these observations seem to indicate the definite increase in the metal particle size and the structural destruction of the graphimet during the heat treatment.

In Chapter III, a simple method is developed in the light of our present experimental results to predict the kinetic parameters of a moderately heterogeneous system by treating each phase independently and combining the effect of each phase together for the net result of the heterogeneous system.

CHAPTER III

THE TEMPERATURE PROGRAMMED DESORPTION/REACTION

APPROACH OF THE GASIFICATION OF CARBON:

THEORY

THE TEMPERATURE PROGRAMMED DESORPTION/REACTION APPROACH
OF THE GASIFICATION OF GRAPHITE: THEORY

A. Theory

We consider the following typical experimental situation for the theoretical considerations of TPD. The carrier gas, usually helium, flows through the uniformly granular catalyst bed at a constant flow rate, while the temperature of the system is linearly raised with time. For the sake of the mathematical simplicity, the following conditions are further assumed:

- (1) Intradiffusion within the catalyst bed is negligible, and the readsorption of desorbed surface species is negligible by maintaining a relatively high carrier gas flow rate.
- (2) Gas molecules (oxygen) dissociatively adsorb on the surface of metal (platinum) particles during the controlled chemisorption, and do not combine with carbon until the metal become active at elevated temperatures. Gas molecules that adsorb on the surface of graphite form surface oxides during the controlled chemisorption at room temperature, T_0 .
- (3) The effective surface areas of graphite and metal, S_c and S_m respectively, are time invariant during heating, and the desorption kinetics of carbon oxides from one surface is not affected by that from the other surface.

- (4) Homogeneity of graphite and metal surfaces is also assumed, and the activation energies of desorption from graphite and metal, E_c and E_m respectively, are independent of coverage.
- (5) A first order desorption is assumed.
- (6) The metal oxide reduction reaction to form carbon oxides is not rate determining.
- (7) The production of carbon monoxide, CO, is dominant, and that of carbon dioxide, CO₂, is neglected.
- (8) The Arrhenius rate expression adequately describes the desorption kinetics, and the frequency factors assume a constant value at 10^{13} sec^{-1} .

A schematic picture of the theoretical system is given in Figure (III-1).

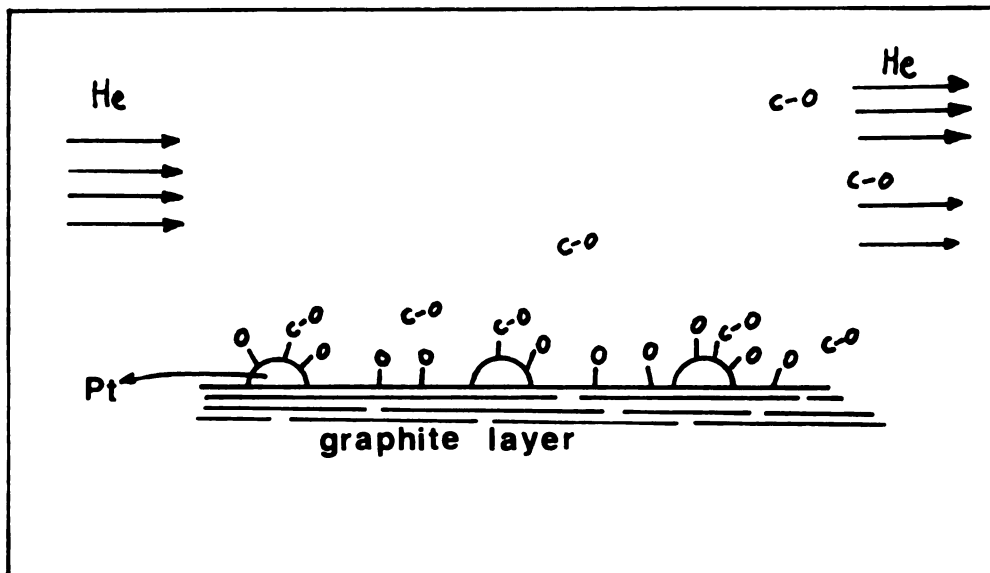


Figure III-1 Schematic Sketch of TFD System

The material balance of CO in the system is given by

$$\begin{aligned} \frac{dn_{\text{CO}}}{dt} &= F_{\text{CO},\text{in}} - F_{\text{CO},\text{out}} + \text{rate of CO production} \\ &= 0 - C_{\text{CO}} Q + SR_{\text{CO}} \end{aligned} \quad (\text{III-1})$$

Assuming no accumulation of CO in the system,

$$\frac{dn_{\text{CO}}}{dt} = 0, \quad SR_{\text{CO}} = C_{\text{CO}} Q \quad (\text{III-2})$$

The production of CO originates from two sources, viz,

- a) active sites on carbon surface, usually edges, and
- b) active sites at the metal-carbon interface.

Hence,

$$\begin{aligned} SR_{\text{CO}} &= S_{\text{C}} R_{\text{CO}}^{\text{C}} + S_{\text{m}} R_{\text{CO}}^{\text{m}} \\ &= S_{\text{C}} A_{\text{C}} \exp(-E_{\text{C}}/RT) \hat{n}_{\text{CO}}^{\text{C}} + S_{\text{m}} A_{\text{m}} \exp(-E_{\text{m}}/RT) \hat{n}_{\text{CO}}^{\text{m}} \end{aligned} \quad (\text{III-3})$$

1. TPD of pure carbon surface (or pure metal surface)

Since $S_{\text{m}} = 0$,

$$SR_{\text{CO}} = S_{\text{C}} R_{\text{CO}}^{\text{C}} = S_{\text{C}} A_{\text{C}} \exp(-E_{\text{C}}/RT) \hat{n}_{\text{CO}}^{\text{C}} \quad (\text{III-4})$$

The peak temperatures of TPD spectra are obtained when the production rate of CO is maximum.

$$\begin{aligned} \frac{d}{dt} (S_{\text{C}} R_{\text{CO}}^{\text{C}}) &= S_{\text{C}} R_{\text{CO}}^{\text{C}} \left[\beta \frac{E_{\text{C}}}{RT^2} - A_{\text{C}} \exp(-E_{\text{C}}/RT) \right] \\ &= 0 \end{aligned} \quad (\text{III-5})$$

Therefore, at the peak temperature,

$$2 \ln T_M^C - \ln \beta = \frac{E_C}{RT_M^C} + \ln\left(\frac{E_C}{A_C R}\right), \quad (\text{III-6})$$

which is the same form as Equation (I-1). There are two unknowns in this equation, viz, E_C and A_C . If A_C can be assumed to be approximately 10^{13} sec^{-1} , E_C is uniquely determined from one experimental T_M . On the other hand, E_C and A_C can be directly determined by considering the inflection point(s) of TPD spectra as well.

$$\text{When } \frac{d^2}{dt^2} (S_C R_{CO}^C) = 0,$$

$$\begin{aligned} \frac{E_C}{R(T_i^C)^2} \left[\frac{2}{T_i^C} + A_C \exp(-E_C/RT_i^C) \right] \\ = \left[\frac{E_C}{R(T_i^C)^2} - A_C \exp(-E_C/RT_i^C) \right]^2 \end{aligned} \quad (\text{III-7})$$

Equations (III-6) and (III-7) can be simultaneously solved for unique E_C and A_C .

2. TPD of Metal Catalyzed Carbon

At the peak temperature, T_M ,

$$\begin{aligned} \frac{d}{dt} (S R_{CO}) &= S_C R_{CO}^C \left(\frac{E_C}{RT_M^2} - \exp(-E_C/RT_M) A_C \right) \\ &\quad + S_m R_{CO}^m \left(\frac{E_m}{RT_M^2} - \exp(-E_m/RT_M) A_m \right) \\ &= 0 \end{aligned} \quad (\text{III-8})$$

Unlike the single site case, the peak temperatures do not necessarily relate to the activation energy of desorption of either carbon or metal. If indeed a first order desorption exists on both carbon and metal surfaces and the activation energies of desorption are independent of coverage, the TPD spectrum of carbon/metal system will be the sum of that of each separate surface, and the shape of the resulting TPD spectrum will depend on the relative magnitudes of E_m and E_c , A_m and A_c , and S_m and S_c .

3. Determination of TPD Spectra of Carbon-Metal System

The rate of CO dissipation in the carbon phase is given by

$$\begin{aligned} \frac{d}{dt} (S_c n_{CO}^c) &= - S_c A_c \exp(-E_c/RT) \hat{n}_{CO}^c \\ &= - S_c k_c \exp[\gamma_c (1 - T_0/T)] \hat{n}_{CO}^c \end{aligned} \quad (\text{III-9})$$

where $\gamma_c = E_c/RT_0$, and

$$k_c = A_c \exp(-\gamma_c)$$

And the following transformation is further carried out.

$$v = T/T_0, \quad v \geq 1$$

$$u_{CO}^c = n_{CO}^c/n_{CO}^c(1), \quad \text{where } n_{CO}^c(1) = n_{CO}^c \text{ at } v = 1$$

$$\bar{\beta} = dv/dt = \beta/T_0$$

Then Equation (II-9) reduces to

$$\frac{du_{CO}^c}{dv} = \frac{-k_c}{\beta} \exp \left[\gamma_c \left(1 - \frac{1}{v} \right) \right] u_{CO}^c \quad (\text{III-10})$$

$$\text{where } u_{CO}^c(1) = 1$$

By the same analogy, the rate of CO dissipation in the metal phase is given by

$$\frac{du_{CO}^m}{dv} = - \frac{k_m}{\beta} \exp \left[\gamma_m \left(1 - \frac{1}{v} \right) \right] u_{CO}^m$$

$$\text{where } u_{CO}^m(1) = 1 \quad (\text{III-11})$$

Therefore, by the assumption of first order desorption of CO from both the carbon and the metal phase, the rate of CO appearance in the gas phase is

$$\begin{aligned} \frac{dn_{CO}}{dt} = \dot{n} = S_c k_c \exp \left[\gamma_c \left(1 - \frac{1}{v} \right) \right] \hat{n}_{CO}^c \\ + S_m k_m \exp \left[\gamma_m \left(1 - \frac{1}{v} \right) \right] \hat{n}_{CO}^m \quad (\text{III-12}) \end{aligned}$$

If it is assumed that

$$S_c/S_m \sim \hat{n}_{CO}^c(1)/\hat{n}_{CO}^m(1) \quad ,$$

then $\hat{n}_{CO}^T(1)/\hat{n}_{CO}^m(1) = 1 + S_c/S_m$ and

$$\hat{n}_{CO}^T(1)/\hat{n}_{CO}^c(1) = 1 + S_m/S_c$$

Using this assumption, Equation (III-12) can be rewritten as

$$\frac{\dot{n}}{S_m \hat{n}_{CO}^T (1)} = (S_C/S_m) (1 + S_m/S_C)^{-1} k_C \exp \left[\gamma_C \left(1 - \frac{1}{v} \right) \right] u_{CO}^C + (1 + S_C/S_m)^{-1} k_m \exp \left[\gamma_m \left(1 - \frac{1}{v} \right) \right] u_{CO}^m$$

(III-13)

Equation (III-13) is the final form desired in the determination of TPD spectra of carbon-metal system. Once u_{CO}^C and u_{CO}^m are determined from two first order nonlinear ordinary differential equations, Equations (III-10) and (III-11), using appropriate values for E_C , E_m , A_C , A_m , and $\dot{n}/S_m \hat{n}_{CO}^T (1)$ (Turnover frequency, TOF) can be plotted against v for different values of S_m/S_C (SRATIO).

These plots are shown in Figure (III-2) through (III-9). In those figures, E_C was assumed to be 260 KJ/mole and 270 KJ/mole, typical values for uncatalyzed oxidation of graphite, and E_m was varied along with S_m/S_C . A_C and A_m were assumed to be constant at 10^{13} sec^{-1} , and β was taken to be 10 K/min.

THEORETICAL TPD PLOTS

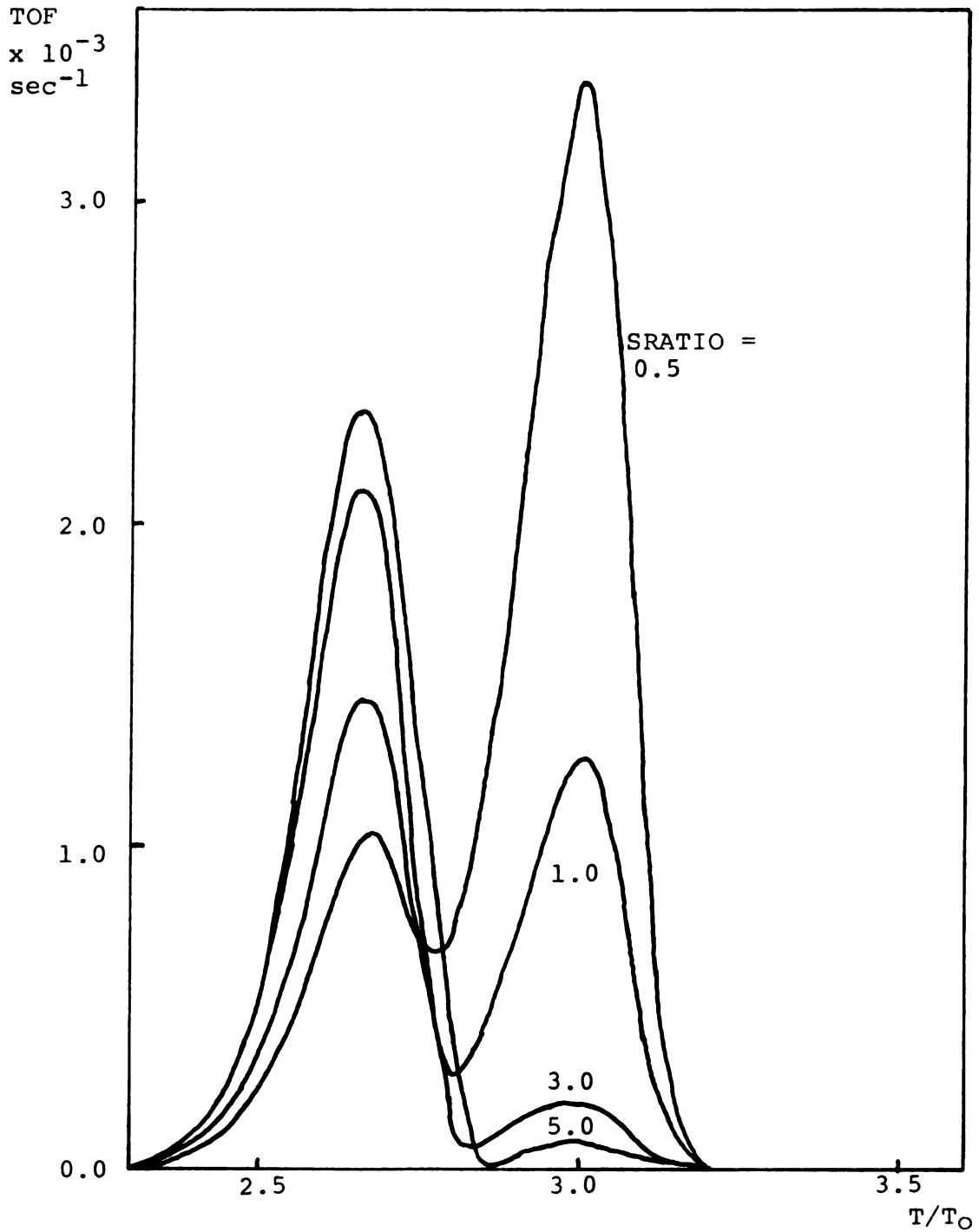


Figure III-2 Theoretical TPD Spectra of Carbon/Metal
 $E_c = 260$ KJ/mole, $E_m = 230$ KJ/mole

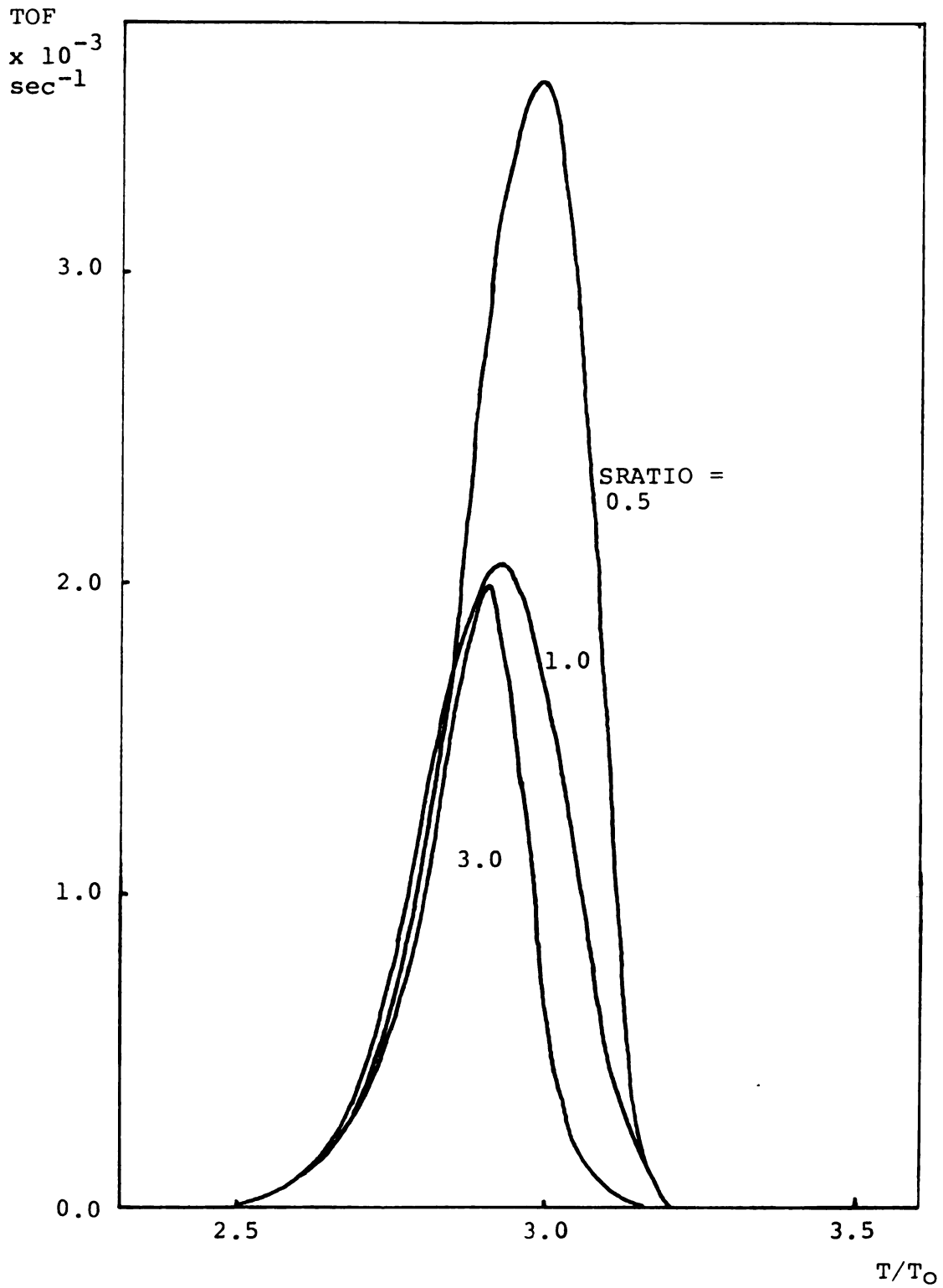


Figure III-3 Theoretical TPD Spectra of
Carbon/Metal
 $E_C = 260$ KJ/mole, $E_M = 250$ KJ/mole

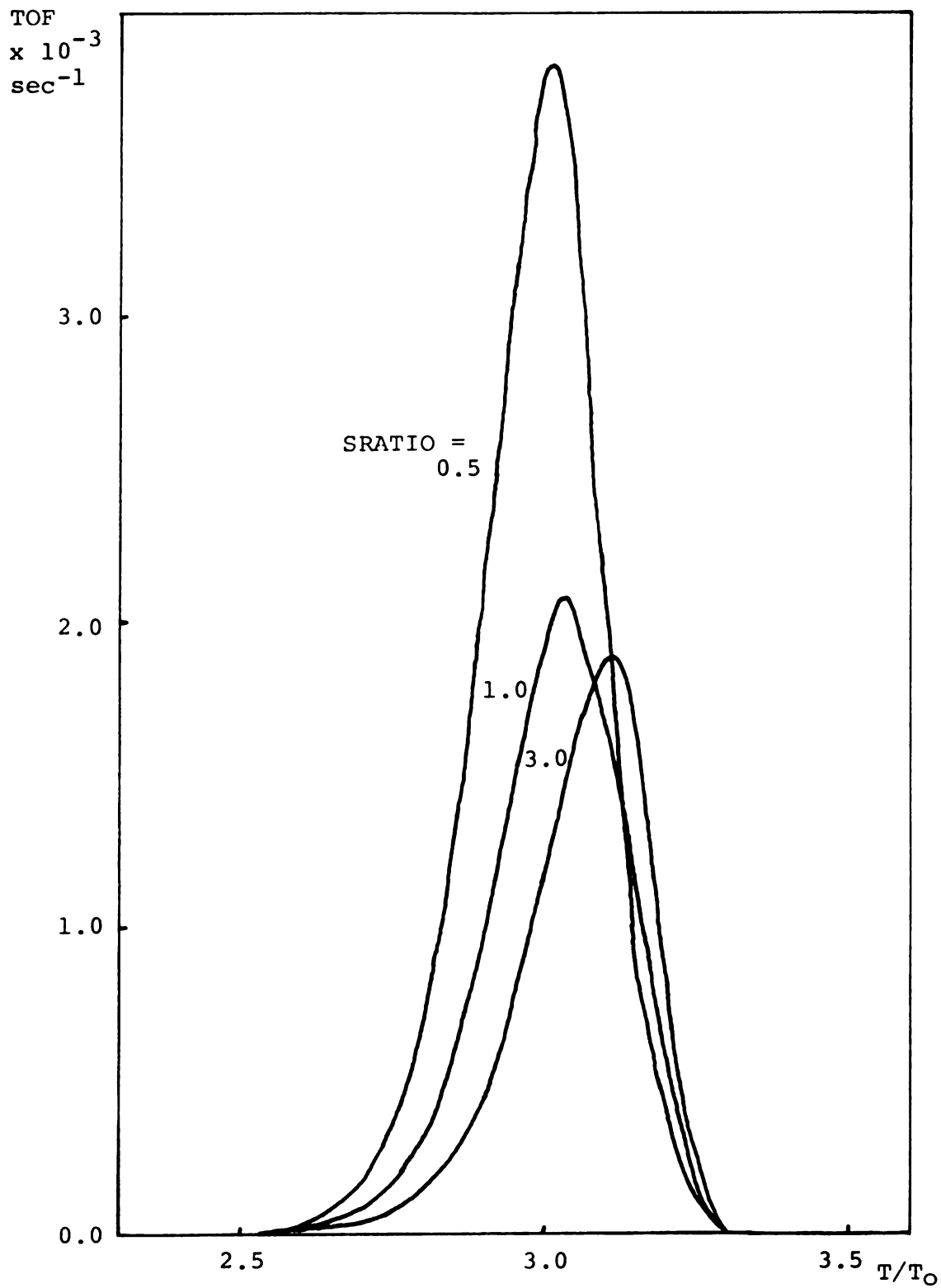


Figure III-4 Theoretical TPD Spectra of Carbon/Metal
 $E_C = 260$ KJ/mole, $E_m = 270$ KJ/mole

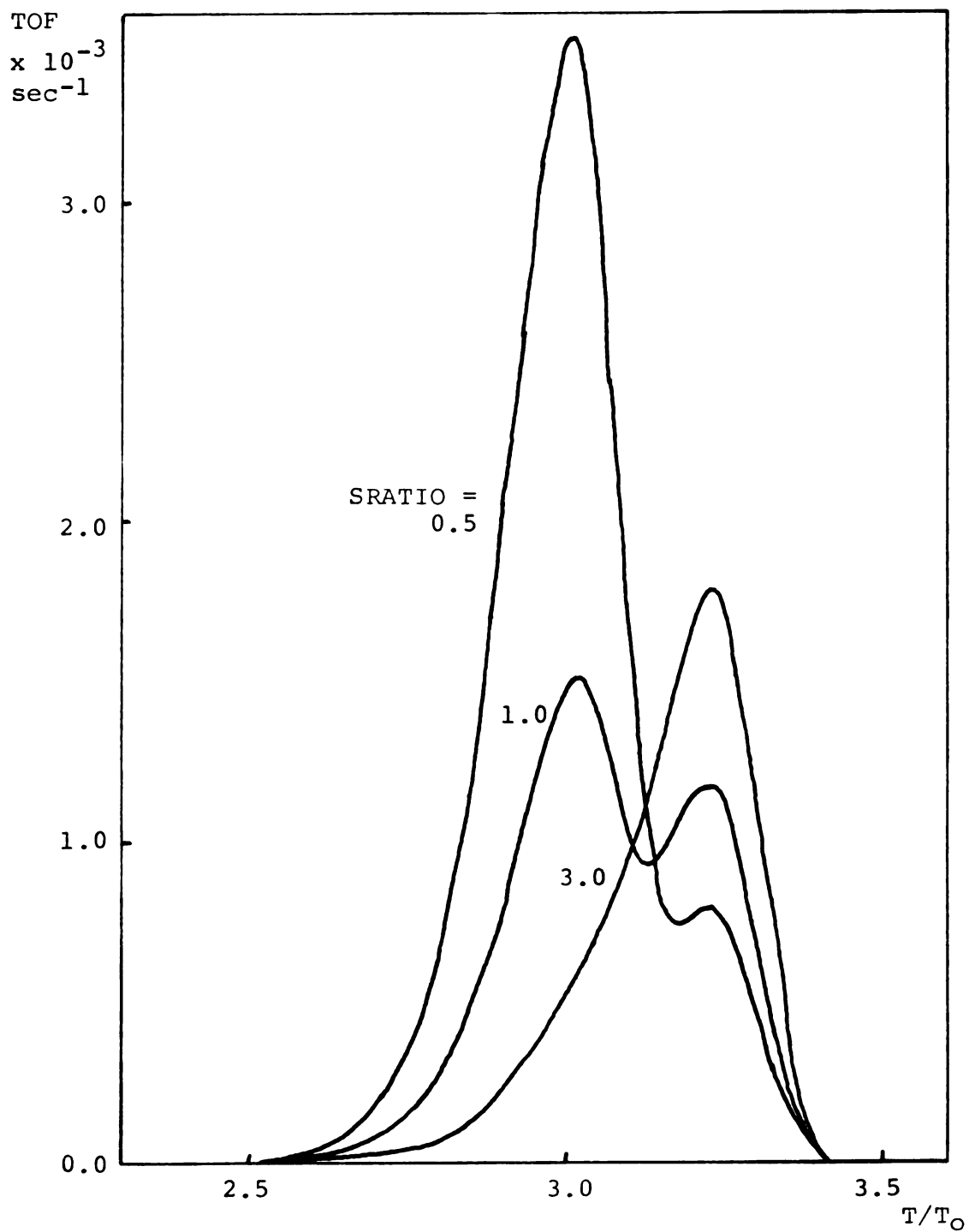


Figure III-5 Theoretical TPD Spectra of
Carbon/Metal
 $E_C = 260$ KJ/mole, $E_M = 280$ KJ/mole

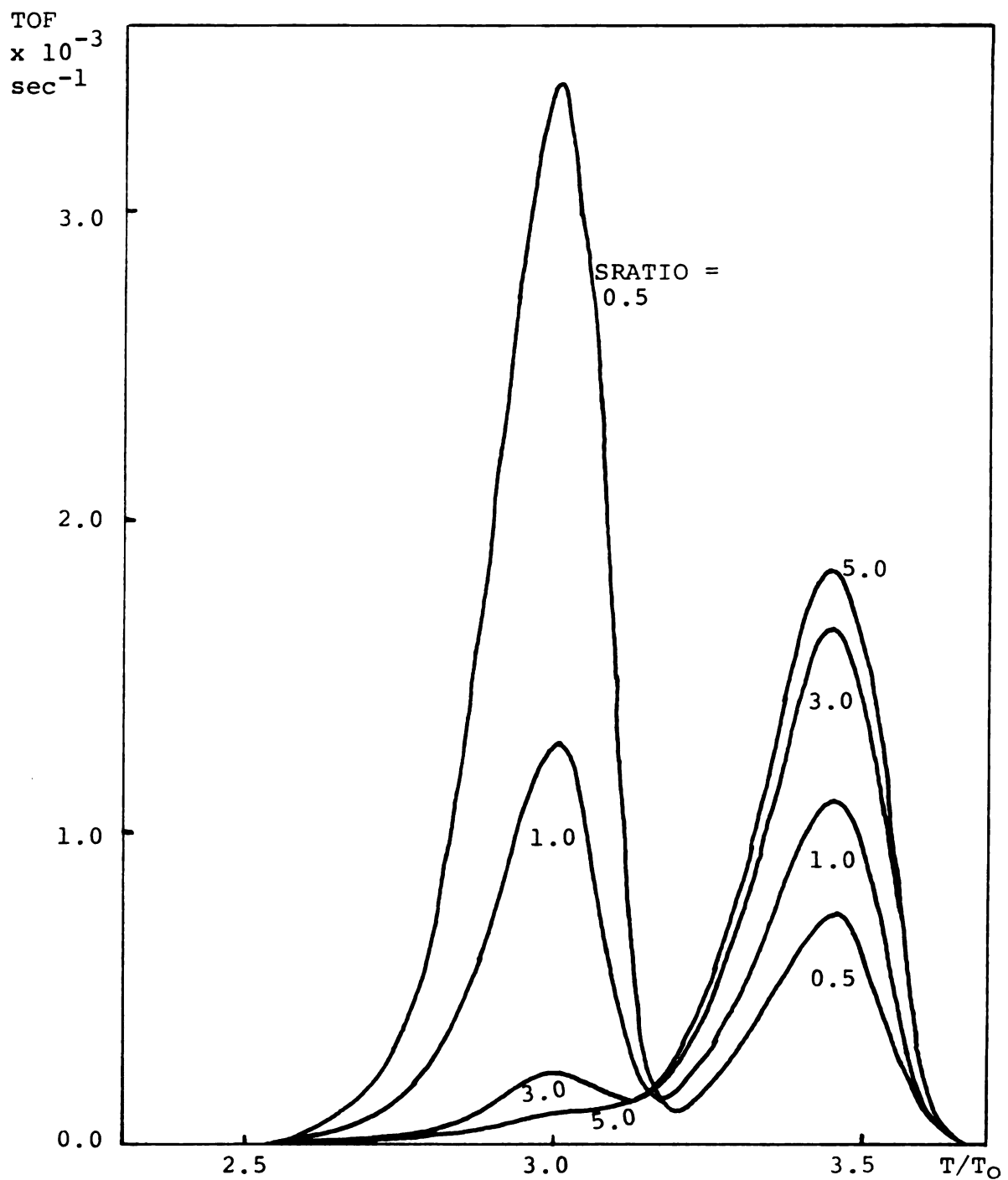


Figure III-6 Theoretical TPD Spectra of Carbon/Metal
 $E_C = 260$ KJ/mole, $E_m = 300$ KJ/mole

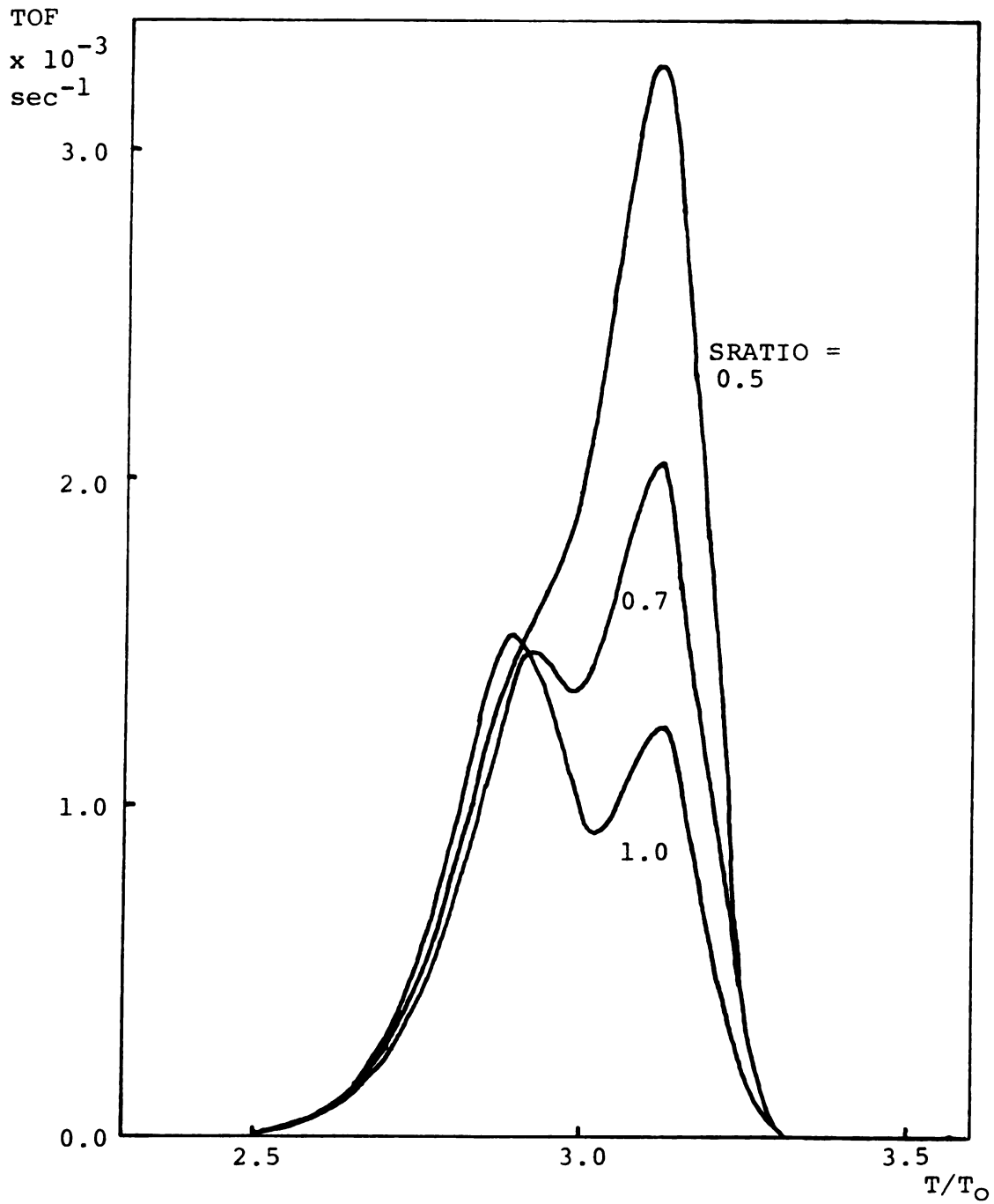


Figure III-7 Theoretical TPD Spectra of Carbon/Metal

$E_C = 270$ KJ/mole, $E_M = 250$ KJ/mole

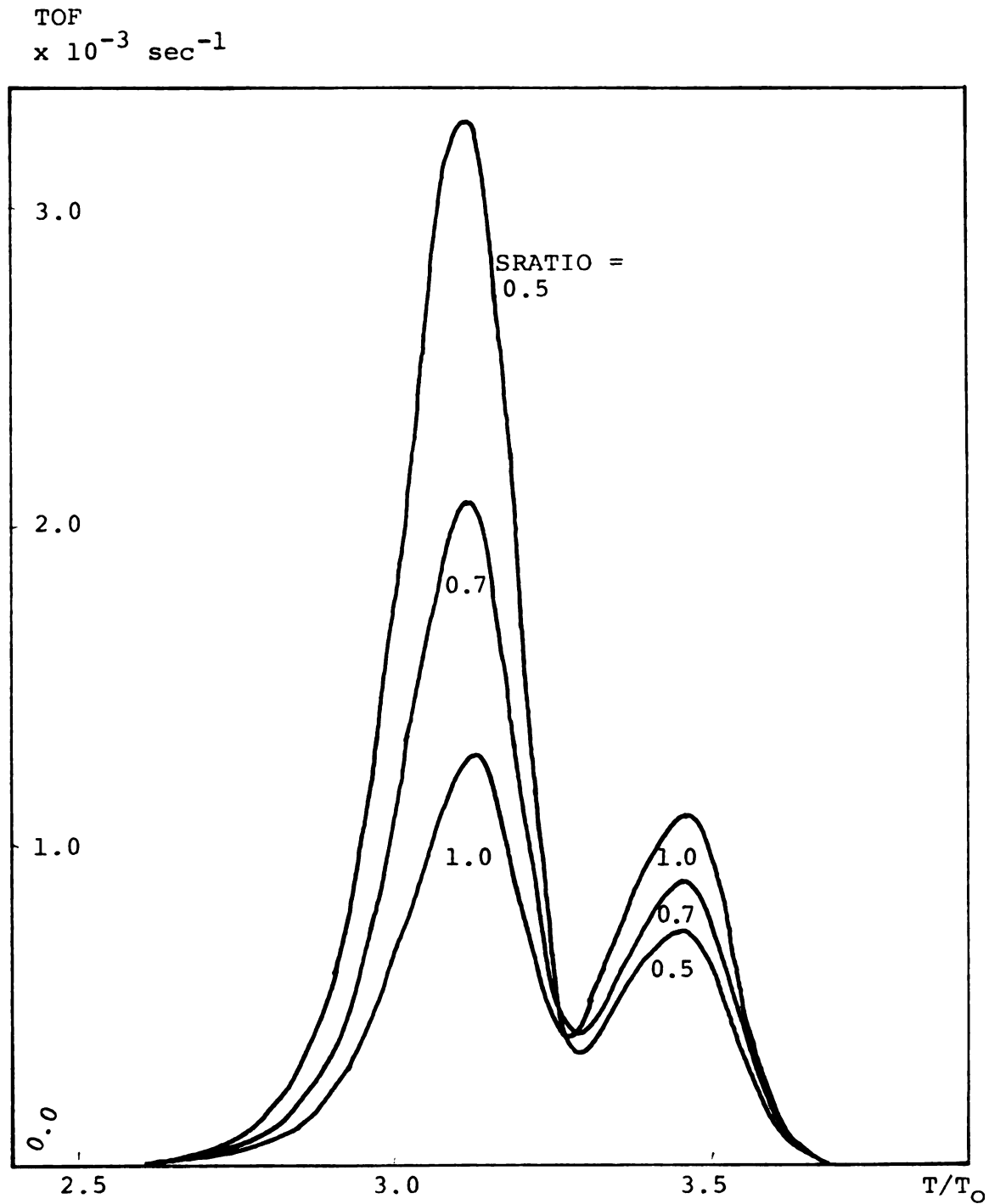


Figure III-8 Theoretical TPD Spectra of Carbon/Metal
 $E_C = 270 \text{ KJ/mole}$, $E_m = 300 \text{ KJ/mole}$

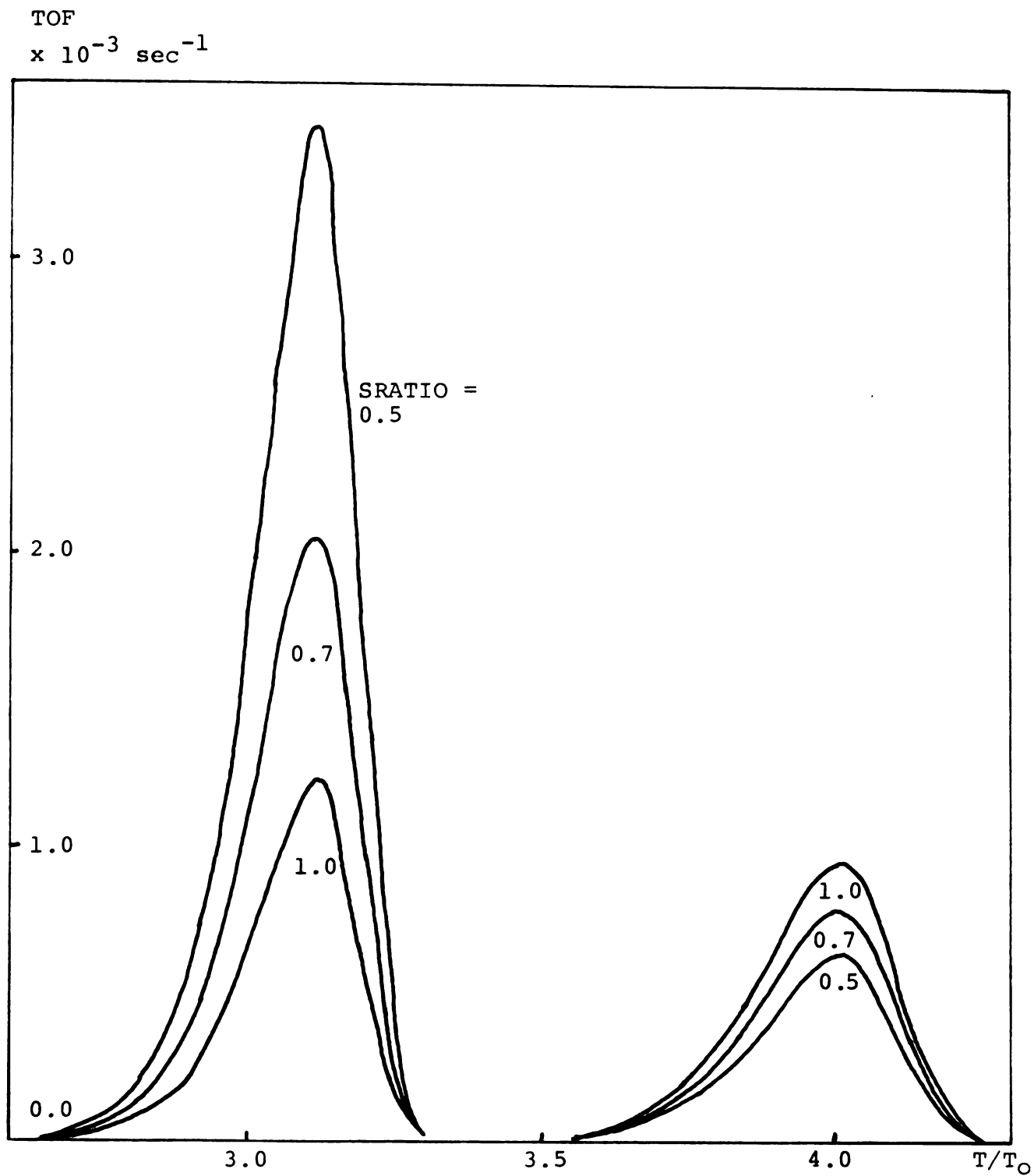


Figure III-9 Theoretical TPD Spectra of Carbon/Metal

$$E_c = 270 \text{ KJ/mole}, E_m = 350 \text{ KJ/mole}$$

C. Discussions on Theoretical TPD Spectra

The surface of the carbon-metal complex is definitely heterogeneous, consisting of the carbon phase and the metal phase dispersed along the graphite layers, but the carbon phase is assumed to have the same characteristics as the pure graphite in the discussion of the theoretical TPD spectra.

For $E_c = 260$ KJ/mole, the peaks of CO spectrum from the carbon phase are always found at $T = 3 T_0$ (Figures III-2, III-5, and III-6), and for $E_c = 270$ KJ/mole, the corresponding peaks are at $3.12 T_0$ (Figures III-7, III-8, and III-9). This implies that the temperature difference of about 40°K changes the activation energy by 10 KJ/mole, and this observation can be used as a method of estimating the activation energy of pseudo one phase in a heterogeneous system.

As can be seen in Figures (III-3) and (III-4), a single peak for CO suggests that the difference between the activation energies of desorption in the metal and the carbon phase is in the range of 10 KJ/mole for all ratios of active sites, and for ratios greater than 3 (Figure III-5) or less than 0.5 (Figure III-7), the difference can be in the range of 20 KJ/mole.

Although the figures were based on the assumption of the negligible readsorption which is unavoidable even in a high vacuum, these differences in activation energies are likely to remain the same, even if the readsorption may influence the desorption from both the carbon and the metal phase.

Since all the peaks for the graphimet were at higher tem-

peratures than those of the pure graphite in the experimental results, it can be concluded from the theory that the activation energy of desorption from the metal phase is greater than that from the carbon phase.

In Figure (III-5), for the ratios of active sites greater than 3, a single peak is expected, but one important aspect of this figure is that for all ratios greater than 3 the peak temperature is the same at $3.25 T_0$, while the experimental peaks shifted to higher temperatures with repeated heating.

If it can be assumed that the surfaces are constantly changing during product desorption and heat treatment, and, so are the ratios of metal to carbon active sites, then the experimental observations suggest that the case where the difference in activation energies is in the range of 20 KJ/mole as shown in Figure (III-5) is not applicable to our experimental results. In Figure (III-4), where the activation energy from the metal phase is 10 KJ/mole greater, the peak temperatures are seen to shift to higher temperatures as the ratio increases. If the active sites are changing upon desorption and heating such that the ratio of metal to carbon active sites increases, this then would be the case adequate to our results.

As discussed earlier, if indeed the annealing of basal plane defects causes the decrease in the active area in the carbon phase, the decrease in the active area due to metal agglomeration has to be less significant in order for the ratio to increase upon heating and subsequent cooling.

Another possible explanation for the increase in the surface area ratio would be due to the opening up of the pore structure upon continued heating thus, allowing the metal particles to be more exposed to gas molecules resulting in an increase in the effective area of the metal. Thus, the total gasification rate increases as well.

Nonetheless, the opposite trend is observed in Figure (III-3) where the peaks shift to higher temperatures as the surface area ratio decreases. This is not applicable to our experimental results since in all cases the peak temperatures are lower than that for graphite. It was shown experimentally with graphite that the peak shifted to lower temperatures with repeated heating. The opposite trend observed in the graphimet sample suggests the following. A shift towards the higher peak temperature indicate a much larger contribution of the metal. Hence this further supports our contention that practically for all cases the ratio, S_m/S_c is increased.

The gasification rate can be affected by the catalysts in two ways, namely, the activation energy and the preexponential factor. In the theoretical argument presented in this chapter the rate was expressed in terms of unit area of active sites, while the preexponential factor was held constant with varying active sites. Hence, the catalytic effect as viewed from the rate expression is represented by either a decrease in activation energy or an increase in the active sites. A typical difference between the peak temperature of graphite and that of

graphimet was experimentally shown to be about 60°K (Figures II-4A and II-8A), and this corresponds to a difference of 15 KJ/mole in the activation energy, which is about 5% of the reported value for graphite. This increase is well within the experimental error, or may have been caused by the apparent lowering of the diffusional barriers as discussed in Chapter II.

If indeed this was the case, the increased gasification rate observed in the graphimet sample must have been due to the increase in the active surface area with little or no change in the activation energy. According to our argument this is true only if the active sites are changing upon repeated heating such that the ratio of the metal sites to the carbon sites is increasing, as depicted in Figure (III-4).

Cases have, in fact, been reported (31) where the activation energies for the catalyzed and uncatalyzed gasifications were the same in spite of large differences in the overall rates. McKee (32) suggested from this observation that the effect of the catalysis was to increase the preexponential factor of the rate equation, which would be the expected result of the rate equation, which would be the expected result of an increase in the density of reaction sites on the carbon surface. He also concluded that a real reduction in activation energy, as distinct from a decrease due to mass transport limitations, would imply that the catalyst effectively increases the rate of the limiting step in the reaction sequence.

Many of these experimental observation on the apparent

activation energy and the preexponential factor were explained in terms of the compensation effect (33), but no satisfactory answer concerning the influences of catalysts on the kinetic parameters of the uncatalyzed reaction has been given since several important variables such as mass- and heat transfer limitations and continuous changes on the gasified surface were neglected.

The simple theory presented in this chapter seems to work fairly well in estimating the relative magnitudes of activation energies and the changes in the active sites of a moderately heterogeneous system during gasification. One improvement that can be readily made on this theory would be to incorporate some kind of functional dependency of the activation energy on coverage, in addition to the already added heterogeneity by treating each phase separately. Amenomiya and Cvetanovic (2) assumed that the composite activation energy was a simple linear function of surface coverage with an upper and lower limit, and obtained theoretical TPD spectra with a much broader peak than that of constant activation energy.

With these kinds of further improvements on the heterogeneity incorporated into the present theory, an interpretation of good experimental results will bear a lot more meaningful details to help us for the better understanding of the mechanism.

CHAPTER IV

THE CHANNEL PROPAGATION RATE OF PLATINUM ON A CARBON SURFACE
A MODEL AND STEM STUDIES

BACKGROUND

Over the past decades, a considerable amount of information has been collected on the catalytic influence of metals on the gasification of carbon under various conditions. It is not until recently that some details of the catalytic activity of these metals have been investigated. Optical microscopy and most importantly, Controlled Atmosphere Electron Microscopy (CAEM) has allowed a detailed picture of the activity of metal catalyst undergoing reactions. The catalytic influence of platinum (27, 34, 35, 36, 37) on the oxidation of graphite has been reported previously. Presland and Hedley (35) used electron microscopy to investigate the Pt/graphite-oxygen reaction at 600-1,000°C, and found that the metal particles were only active as long as they contacted edges or steps on the graphite surface. Some particles produced pits while others generated channels across the surface. L'Homme et al. (36) investigated the same reaction and suggested that oxygen dissociated on the platinum surface and the atoms produced migrated over the catalyst particle to the carbon. Just recently, Baker et al. (16) investigated the catalytic oxidation of graphite by platinum employing CAEM. In their study, they found that at 500°C, the average particle size grew and in some instances were penetrating the graphite basal plane to produce pits. The pits were subsequently expanded by edge recession due to the uncatalyzed attack and thereby producing hexagonal

holes. However, upon continued oxidation, the pit increased in depth and the uppermost graphite layers become progressively more circular in shape.

At 735°C, another mode of catalytic attack was occurring. Those particles which had previously created pits initiated an action parallel to the basal plane to form channels, with the particle at the head of the channel. They have also observed that channels were also being produced by other particles which had contacted edges or steps on the graphite surface. With respect to the particle mobility, channels propagated by small particles (up to 25 nm diameter), were relatively straight lines, making angles of 60° and 120° to one another, and were usually oriented parallel to the $(11\bar{2}0)$ directions. Particles greater than 100 nm diameter propagated irregular channels, which possessed hexagonal facets at the graphite-catalyst interface. Here the facets are oriented parallel to the $(11\bar{2}0)$ directions.

some interesting behaviour of the particles were also observed and are common to all channeling particles:

- (1) The width of the channel was dictated by that of the catalyst particle responsible for its propagation, and often changed as the particle spread or contracted at the graphite-metal surface.
- (2) In some instance, the particles break and the fragmentary particles continued to channel but at a faster linear rates than that of the progenitor. Conversely,

active particles collided with inactive stationary particles and coalescence occurred. At this instance, the channel propagation was arrested for a brief time, and finally the new particle accelerated to reach a new but lower constant channel propagation rate.

- (3) Loss of activity occurred if the particle lost contact with an edge on the graphite surface. At higher temperatures, such particles often contained sufficient kinetic energy for motion to locate a fresh edge or step and continued to propagate channels.
- (4) A spherical form is assumed by particles which temporarily lost their activity (i.e., mobility). In contrast, inactive particles, which remained stationary, were irregularly shaped. At 850° C, there was general particle mobility and all particles became spherical in form.

A striking observation was found by Baker et al. (16) in relation to channel propagation rate and particle size. Their quantitative kinetic analysis showed that for a given temperature, the linear rate of channel propagation was inversely proportional to both the catalyst particle size and the channel depth. It is the purpose of this section to prove some of these effects by a model.

SCANNING-TRANSMISSION ELECTRON MICROSCOPY OF
UNREACTED AND REACTED PLATINUM GRAPHIMET

Here, we briefly present some of the electron microscopies of both unreacted and reacted platinum graphimet. Since Baker's experiment used a different system, viz, platinum evaporated on a single crystal graphite (from Ticonderoga) and platinum (from drying of chloroplatinic acid) on a single crystal graphite, we investigated the behaviour of platinum particles for graphimet, and then determine if there is suitable agreement with Baker's results.

Figures (IV-1) to (IV-4) show a scanning transmission spectroscopy of an unreacted platinum graphimet. All the electron micrographs use the bright field emission from a STEM (Model HB 501 by VG Instruments, Inc.).

Figure (IV-1) is a 100,000 magnification ($1,000 \text{ \AA}/\text{cm}$) of a graphimet flake situated on a holey film on a copper grid. Clearly, the graphimet we obtained from Alfa Corporation is not purely an intercalated one but instead, represents a combination of very highly dispersed platinum and large clusters of smaller groups of platinum. The platinum shown as highly dispersed and clustered particles are verified by using an X-ray dispersive analyzer. Some dark points within the specimen, represented copper and this was verified by having a very high correlation from X-ray analysis for copper as shown in Figure (IV-5). For instance, in Figure (IV-1), sections

D and E represent copper. This is not surprising because the background used was a copper grid, and it was very difficult either to prevent during the sample preparation the tearing of the plastic holey film or placing snugly miniscales of graphimet flakes within the boundaries of the copper grid. Furthermore, the hybridization of transmission electron microscopy with scanning electron microscopy allows to show the depth profile of the specimen.

Hence, a slight opening of the graphite flakes can be visibly detected by the scanning mode.

Our observations on the unreacted graphimet support the findings of Smith et al. (38). Their observations reveals that the intercalated element was present primarily as small islands of either metal or metal oxide on the surfaces of their graphite flakes which appeared to have been separated as a consequence of the manufacturing procedure. In order to obtain a yet better resolution of the particles, we increased the magnification of a certain section in Figure (IV-1), section A.

Figure (IV-2) is an expanded view of section A with a 500,000 magnification ($500 \overset{\circ}{\text{Å}}/\text{cm}$). Here, we notice the clusters of particles having sizes in the order of about $20 \overset{\circ}{\text{Å}}$. Another striking feature of this photograph is that fringes can be visibly seen. These lattice fringes arise from openings between graphite planes which contain some clusters of platinum (Section G, Figure (IV-4)). This prompted us to further increase the magnification and examine the platinum intercalates. Figures

(IV-3) and (IV-4) show a 10^6 ($5\text{\AA}/\text{cm}$) and 2×10^6 ($2\text{\AA}/\text{cm}$) magnification of section B. Note the lattice fringes have become more visible. All dark and somewhat round spots were identified as platinum, using again the X-ray dispersive analyzer. For all sections of the platinum graphimet investigated, all showed small and large clusters of platinum.

There are two findings that revealed by these micrographs which have not yet reported in the literature. First, the platinum graphimet, aside from not being an intercalated specimen, contains small amounts of impurity. For the sample used, X-ray dispersive analysis detects low levels of chlorine and iron. Although it is not reported here, other sections in the specimen reveal the presence of small amounts of silicon. In all TPR and TPD experiments it was assumed that at these low levels, the impurities do not impart any other catalytic activity. This is rightly so for the following reasons. Silicon is catalytically inactive and probably will not form an unreactive Pt-Si phase. Chlorine can be removed during the successive pretreatment with oxygen. Although iron processes a catalytic activity in the steam/ H_2 gasification of graphite, a pre-exposure with oxygen and conducting a series of similar pretreatments will enable iron to form a more stable but unreactive iron oxide. Second, in contrast to the findings of Fisher et al. (38), it was observed that the islands of platinum which are very small are not less numerous. However, other micrographs confirm Fisher et al.'s findings that there is a

tendency of the particles to cluster along crevices between two overlapping flakes (Section F in Figure (IV-1)), or at surface steps, although there did not appear to be any preferred orientation of the platinum lattice planes relative to that of the graphite.

The electron micrographs for the reacted platinum graphimet do not resemble those of the unreacted. Here, the reacted platinum graphimet is referred to as the sample which had undergone the temperature programmed desorption/reaction as described in the Chapter II. In all the electron microscopies of the platinum graphimet flakes, it is observed that the platinum particles tend to be more spherical as was also observed by Baker et al. (16). Furthermore, the particles are more organized and are not highly dispersed into small islands as that found for the unreacted sample. It can thus be speculated that during the few minutes of ramping of the temperature (after pre-exposure to oxygen), the highly dispersed platinum islands become mobile and agglomerate (or sinter) to form larger particles. In the TPD/TPR set-up, the sintering occurred in the absence of an external oxygen flow, in contrast to the experiment of Baker et al. (16), where 1 torr of oxygen was flowed continuously over the Pt-graphite. Figure (IV-6) is a STEM of a reacted platinum graphimet with a 50,000 magnification ($2,000 \text{ \AA}/\text{cm}$). A number of possible catalytic activities can be conjectured from this electron micrograph. Clearly, particle channeling is one such catalytic activity.

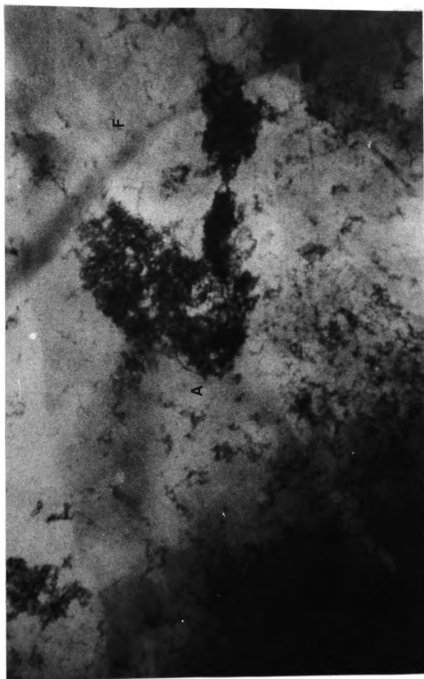


Figure IV-1 STEM of unreacted Pt-graphimnet (1,000 Å/cm)

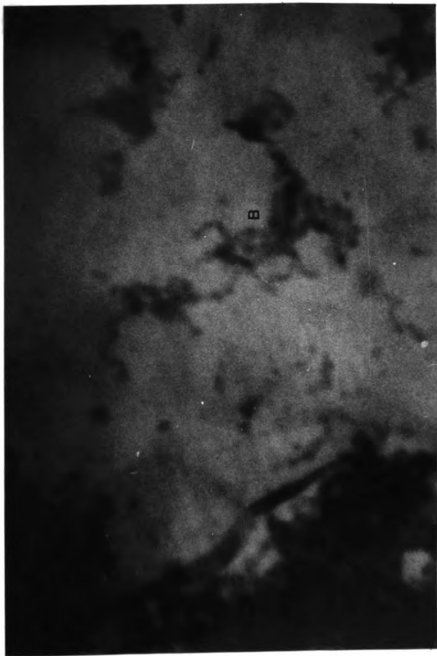


Figure IV-2 SITM of unreacted Pt-graphiret (500 Å/cm)

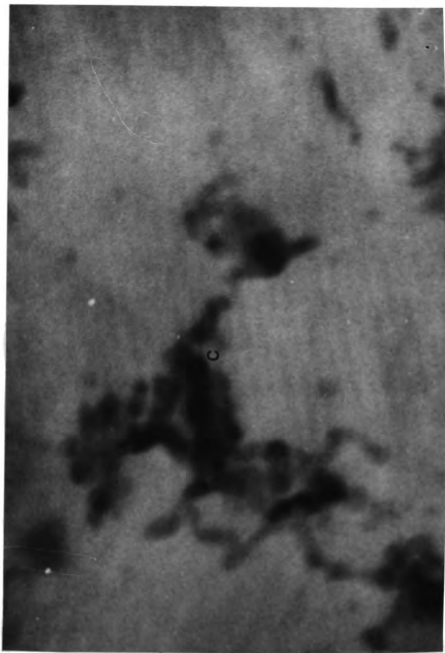


Figure IV-3 STEM of unreacted Pt-graphinet (50 Å/cm)

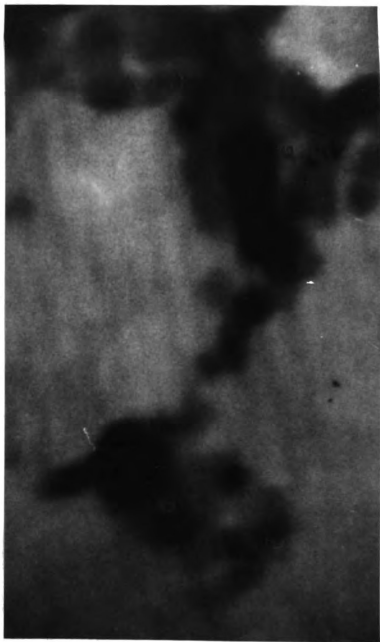


Figure IV-4 STEM of unreacted Pt-graphimnet (20 Å/cm)

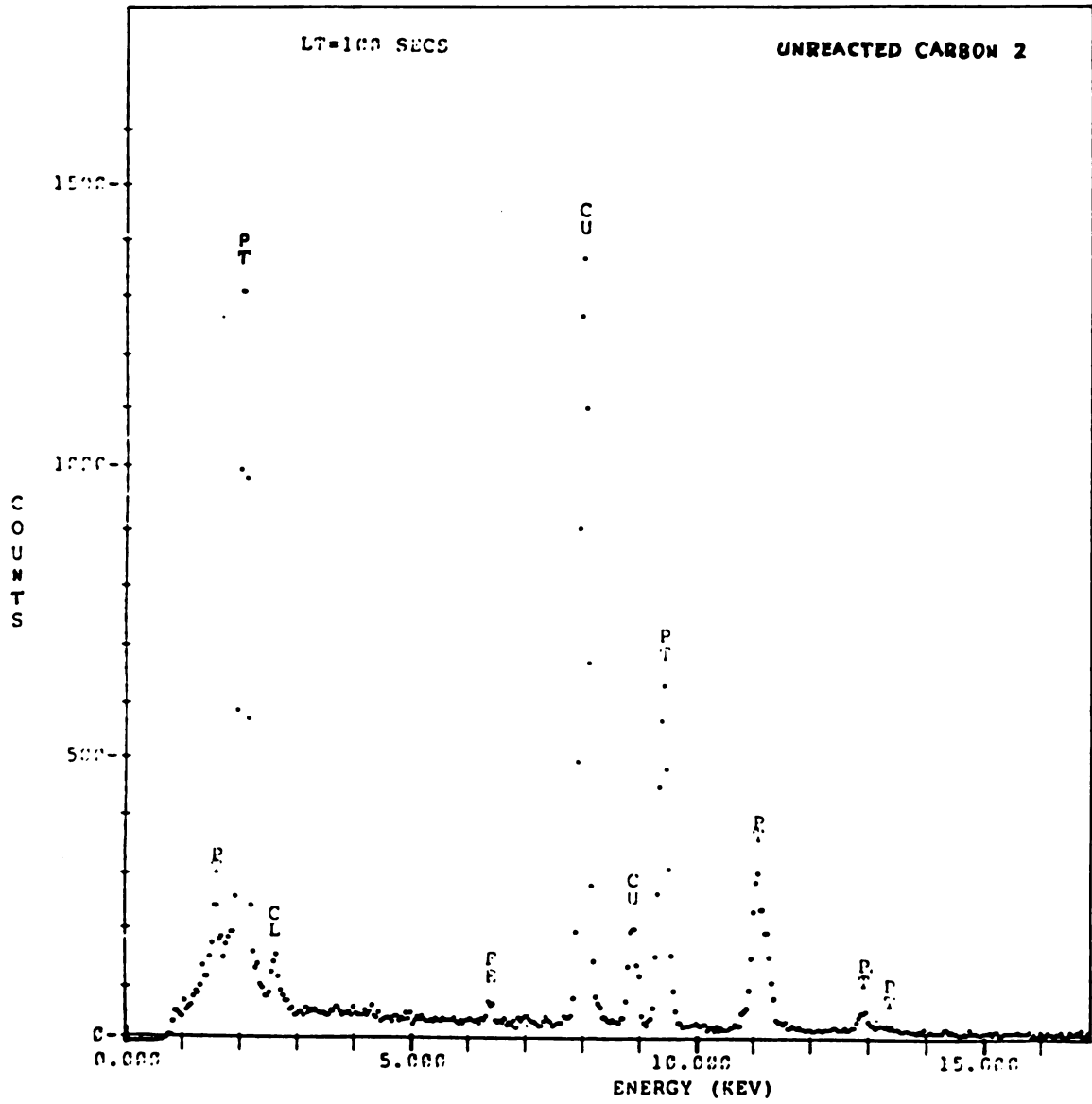


Figure IV-5 X-ray dispersive analysis of Pt-graphinert

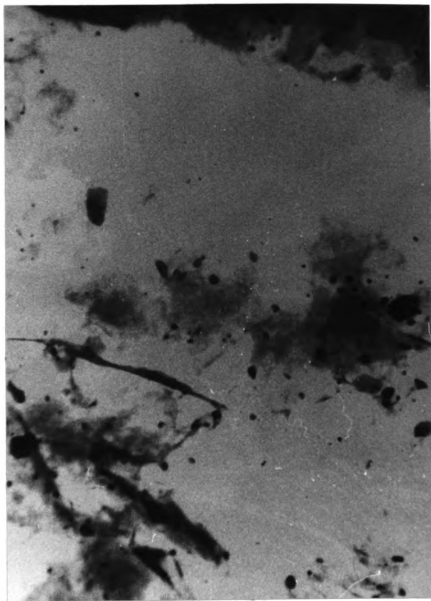


Figure IV-6 STM of reacted Pt-graphinnet ($2,000 \text{ \AA/cm}$)

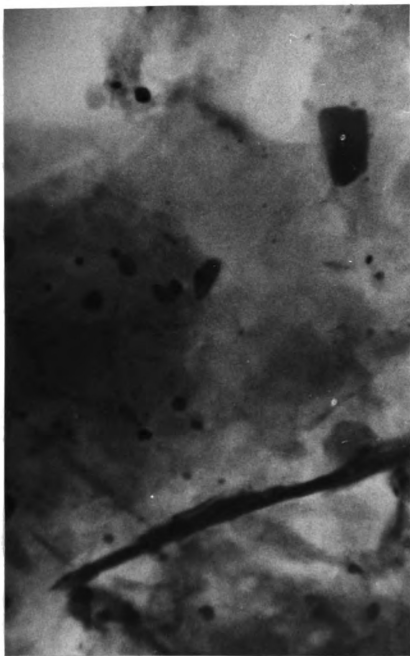


Figure IV-7 STEM of reacted Pt-graphimict (1,000 Å/cm)

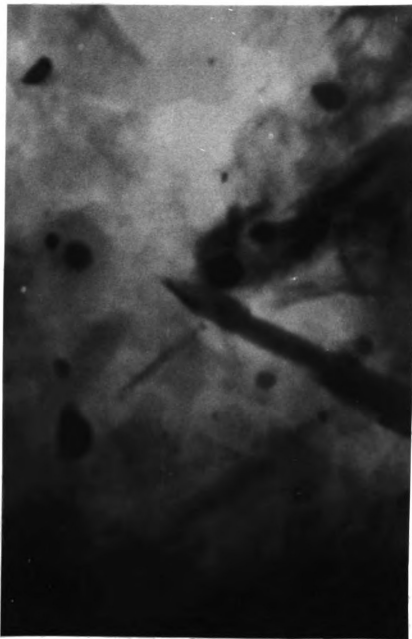


Figure IV-8 STEM of reacted Pt-graphimnet (500 Å/cm)

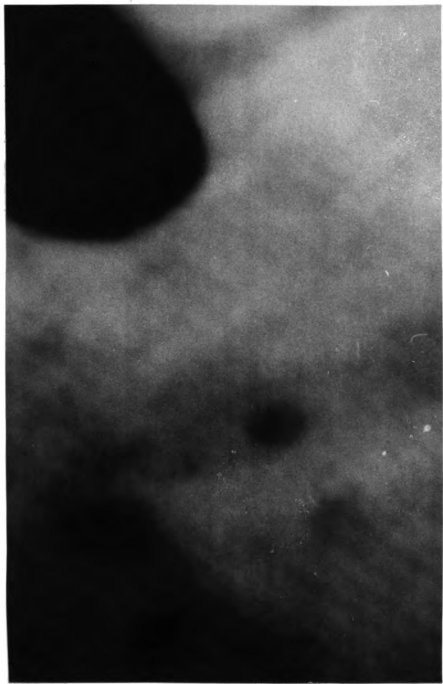


Figure IV-9 STEM of reacted Pt-graphinnet (100 Å/cm)

Figures (IV-7) and (IV-8) are a 100,000 and 200,000 magnifications respectively of the same platinum graphimet flake. The narrow channel runs from the middle upper left to the lower left portion of the picture. X-ray dispersive analysis reveals that the channels do not contain any platinum except near the end points. The Figure (IV-10) illustrates more clearly the situation. Platinum particles within the channel have sizes ranging from about 100 to 150 Å. To the right of the narrow channel is another channel. However, this channel is wider but shorter and contains a larger platinum particle (~375 Å). This observation was also made by Baker et al (16), where larger particles tended to have slower propagation rate than smaller particles.

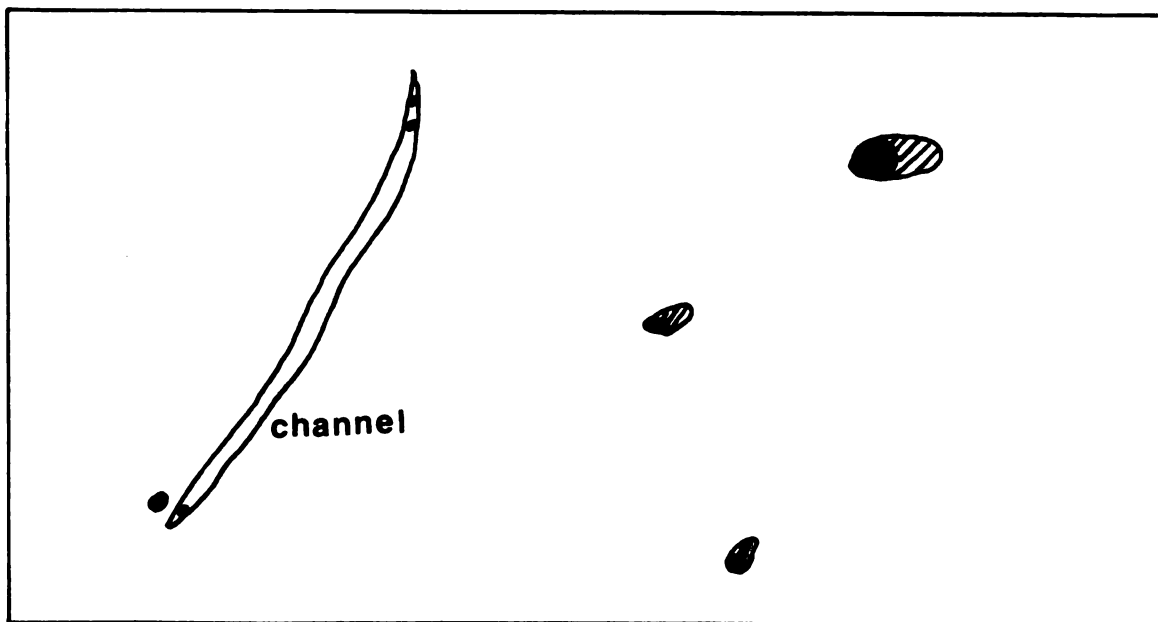


Figure IV-10 Schematic Illustration of Various Channelling Activities in Figure (IV-7)

Figure (IV-9) is a one million magnification ($100 \text{ \AA}/\text{cm}$) of the same reacted platinum graphimet. The large dark spot at the upper right corner is platinum (as determined from the X-ray dispersive analyzer) having a particle length of about 400-450 \AA . This electron micrograph shows that the particle did not exhibit a channeling activity. It is also observed the graphite lattices are intact and unaffected by the small gasification activity (because of the low level of oxygen exposure). Although there was no STEM of a reacted graphite such that no direct comparison could be made, it can be summarized however from these electron micrographs that most of the catalytic activity occur within the vicinity of the platinum particles.

Another catalytic activity is the pitting mode. There seem to be no clear distinction from these electron micrographs of such activity and will require specifically a scanning electron microscopy. However, some particles of the electron micrographs reveal somewhat that pitting action might have occurred. The lower left section of Figure (IV-6) probably depicts a relatively good STEM resolution of the pitting mode.

Six conclusive statements can be made in regards to these studies. First, there is a resemblance of catalytic activities between Pt/graphite and platinum graphimet. Hence, it can be hypothesized that such activities could be occurring for other Pt/carbon system, e.g. Pt/char. Second, the TPD/TPR set-up

as describe in Chapter II can be a very viable tool for determining intrinsic kinetic rates of gasification since turnover rates can be calculated on an almost constant surface metal area. This is equivalent to studying the gasification kinetics in a differential mode where low levels of oxygen exposure lead to low conversions. Furthermore, for low conversion, diffusion controlled reaction is almost eliminated, hence we are confident that the activation energy obtained is not apparent but true activation energy. Although this was not discussed earlier, an electron microscopy of the platinum graphimet at various temperature conditions in the TPD/TPR experiment should reveal an almost similar morphology (size and shape) of the platinum particles. This was not executed in this study because of a certain difficulty of the implementation. It is conjectured here that particles first rearrange at lower temperatures even at temperature below any incipient gasification activity. Hence, once a definite morphology is established it would have remained as such until the end of the TPD/TPR run. From this, the assumption of constant metal surface area during that part of the catalytic activity is not far flung. Third, the catalytic activity occurs within the particle's vicinity, thus requiring a good contact between metal and support (carbon). Fourth, platinum can sinter in small amounts of oxygen (from desorption), carbon monoxide and carbon dioxide as reacted by the TPD/TPR experiments and electron microscopy. Hence, metal-support

interactions are not probably strong. However, it is surprising that platinum exhibits good catalytic effectiveness. And furthermore, it was not mentioned earlier that there should be a good contact between metal and support for any catalytic activity to occur. Here, the excellent contact between metal and support is not a measure of SMSI (Strong Metal Support Interactions). It is viewed here that the contact is a result of the catalyst performing a depolymerization or carbon-carbon bond breaking. Boudart and Holstein (14) support such idea. They are rightly so because the hydrogenolysis of carbon-carbon bonds is a limiting process in the hydrogenation of carbon to methane. We speculate that from our data based on TPD/TPR experiments, platinum functions as an agent for carbon-carbon bond breaking. The following argues such validity:

First, assuming (1) a first order rate for both catalyzed and uncatalyzed reaction and (2) the reduction of the metal oxide largely by a carbidic carbon and desorption of surface carbon oxides are not rate limiting, and it is found that the activation energies of the uncatalyzed and catalyzed rates are just slightly different from each other. This implies that the carbon-carbon bond breaking is rate limiting. From the TPD/TPR experiments, the activation energies are 310 KJ/mole and 300 KJ/mole for the catalyzed and uncatalyzed rates, respectively. This also implies here that platinum does not alter the reaction pathway of the uncatalyzed rate. The slight

lowering of the activation energy is usually interpreted as an enhancement of the carbon-carbon bond breaking. Second, from the TPD/TPR spectrum, the incipient gasification (expressed in terms of any surface oxide evolution, mainly carbon dioxide) occurs at a lower temperature (500-510°C) for platinum-graphimmet than graphite (600-620°C). In the conduct of the TPD/TPR experiments, one observation is worth noting. The differences in the temperature at incipient gasification between catalyzed and uncatalyzed rates could be hardly detected from the weight loss data. It would require a very sensitive electrobalance to detect a weight loss in the order of 10^{-9} mole. This was circumvented here by measuring the gas evolution using a sensitive gas chromatograph. Hence, our TPD/TPR experiments reveal that gasification could start at a much lower temperature than what is usually reported in the literature by weight loss data. Thus, platinum acts as an agent for implementing the carbon-carbon bond breaking leading to the formation of a carbon-platinum bond with subsequent reaction of the carbidic carbon with a thin layer of metastable platinum oxide. Here the metastable platinum oxide could consist of a weakly bound oxygen, as envisioned by Holstein and Boudart (15) and perhaps not forming a separate phase in contrast to the suggestions by Baker and Coworkers (17, 18). This leads us to the fifth conclusion. We concur with Baker's suggestion that there is probably a thin layer of metal oxide which could be metastable and becoming non-thermodynamically

or non-stoichiometrically unstable at higher temperatures because of its subsequent reactions with the carbidic carbon. This is supported from the TPD/TPR experiments where both graphite and platinum graphimet were preexposed to equal amounts of oxygen. A weakly bound atomic oxygen on the platinum surface arise from a dissociative chemisorption of oxygen, even at lower temperatures. We have made no verification as to whether atomic oxygen reacts or diffuses within the reduced metal matrix at lower temperatures. The former is very possible on iron surfaces. For longer oxygen exposures diffusion within the platinum crystals is not a remote possibility. At the outset of the temperature ramping, some weakly bound oxygen is desorbed and carried away by the inert gas and the rest of the bound oxygen partake to form the metal oxide during the rearrangement of the particles (e.g. redispersion and sintering) and at which time there is yet no gasification activity. Hence, preceding any gasification activity, the particles could have two phases which are not necessarily distinct and for which the oxide phase is not necessarily a thermodynamically stable metal oxide. Furthermore, at roughly the same initial weights for both graphite and platinum graphimet, the latter has a larger initial oxygen uptake as clearly demonstrated by the total evolution of the surface carbon oxides (CO and CO₂) in the TPD/TPR spectrum (Figure II-4B and II-8B). This suggests that any dissociated oxygen at exposure temperature is nearly maintained intact (except perhaps for small desorption)

until its reaction with a carbidic carbon at elevated temperatures. Moreover, it is evident that in the absence of an external flow of oxygen, a huge level of CO is detected at temperatures greater than 700°C with a lapse time of nearby 80 minutes before the first detection of carbon monoxide. This suggests that a source of oxygen has been kept for the CO production, and it can be conjectured that since there is no other source of oxygen, such oxygen source could have been supplied from an unstable metal oxide layer. The occurrence of atomic desorption of oxygen is probably a remote possibility and if it occurs at all it will be at a minimum level and they have to be desorbed at lower temperatures. However, with the temperature ramped such possibility is virtually nil. Moreover, on the basis of thermodynamic argument, it is almost impossible to reduce Pt-O to Pt + $\frac{1}{2}\text{O}_2$ by a simple heat treatment. Hence, once an oxide is formed at relatively lower temperatures it will remain as such. We believe our TPR/TPD results strongly suggest the existence of a metal oxide layer (be it stable or unstable) and is especially supported by the fact that there is no continuous flow of external oxygen in the TPD/TPR experiments. We are not discounting the existence of a weakly bound oxygen. This is probably present in a continuous flow of oxygen. However, we cannot totally disregard the existence of a thin layer of metal oxide as our TPD/TPR experiments strongly suggest. In the next section of this Chapter, we have set forth a mathematical model which includes

the existence of a thin layer of metal oxide and show that this model supports our theory and that of Baker for it matches those of Baker's (16) data on channelling rate.

Finally, we think that an oxygen transfer mechanism is also operating for the platinum catalysis. This is supported by the following. The activation energies of both catalyzed and uncatalyzed rates are not distinctly different and yet the reaction rate is more than doubled in the former. The enhancement in the catalyzed rate can be explained by a compensation effect (39, 40, 41) where the pre-exponential factor has values much greater for the catalyzed than the uncatalyzed rate. The pre-exponential factor is related to the active sites density. Hence, it is clear that platinum creates and furnishes more active sites density. Otto and co-workers (31) found the same conclusion for the nickel-catalyzed steam gasification of char and pure graphite. Boudart and Holstein (15) seem to support the oxygen transfer mechanism for the oxidation of carbon by transition metals.

Now, Otto and co-workers (31) interpreted the increase in active sites density as due to oxygen transfer rather than by electron transfer. For the latter to occur, they suggest that there should be a substantial decrease in the activation energy for platinum-graphimetric. However, an ease in the breaking of the carbon-carbon bond would imply an increase in the rate of formation of active carbon, thus increasing the number of active sites density which is a compensation effect. Here,

we therefore view the two mechanism, viz, oxygen and electron transfers as totally distinct and so it is possible that both mechanisms are occurring in any gasification of carbon. That the latter is rightly so can be viewed in terms of the viscous metal oxide layer theory we hypothesized earlier. To decipher which mechanism is rate limiting seems to be not clear from our experiments and would require a more detailed kinetic study. One suggestion is to use tracer techniques.

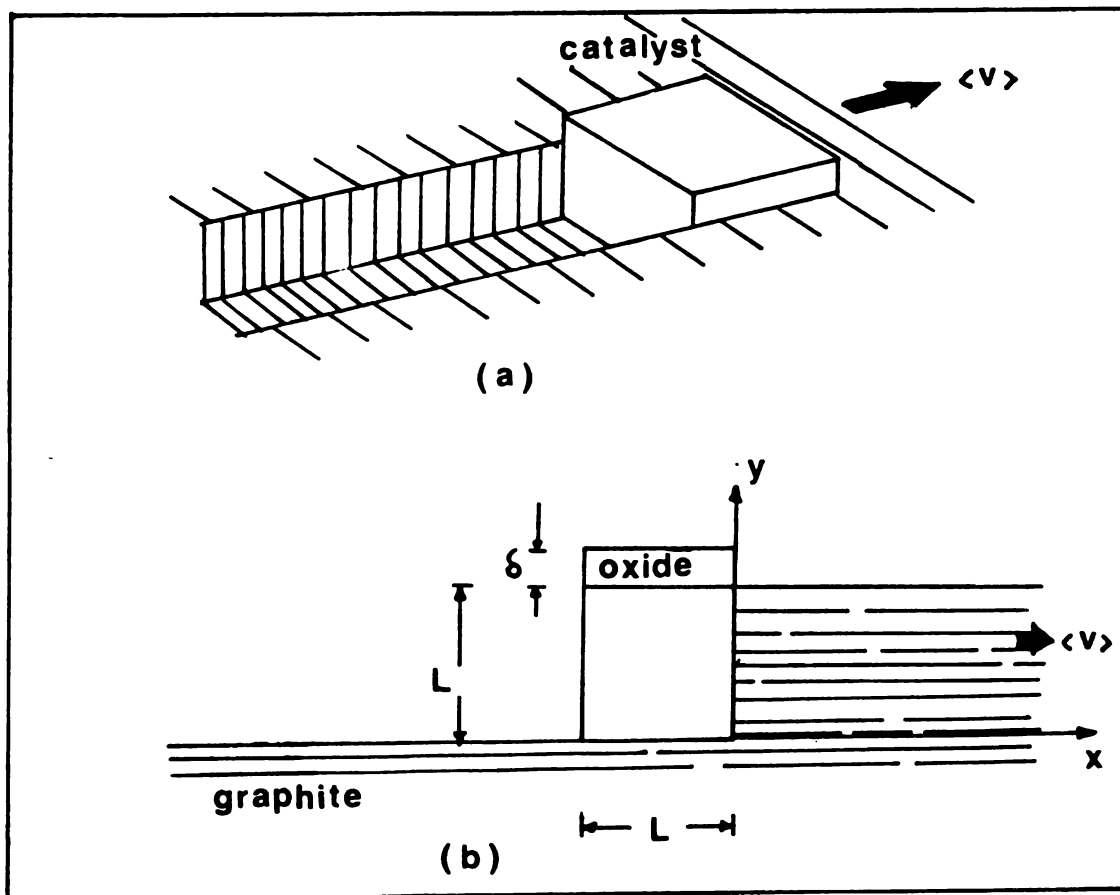


Figure IV-11 Simplified Sketch of Particle Channelling Activity - Model
(a: a general view, b: two dimensional view)

A MATHEMATICAL MODEL
OF THE CATALYST PARTICLE PROPAGATION RATE
DURING AN ACTIVE GASIFICATION OF GRAPHITE

Much has been speculated about the catalyst behaviour during gasification. Crucial to all of this is the existence of a thin viscous layer of metal oxide. Boudart and Holstein (15) hypothesized that since noble metals, which are only present in the reduced state, are able to catalyze the C-O₂ reaction is an evidence that two phases are not needed. Baker and co-workers (17) on the other hand suggests its existence. By measuring the channel propagation rate through the use of CAEM, they have found an underlying distinction between catalyzed oxidation and catalyzed hydrogenation. In the former, the rate at which particles propagate or create channels is inversely proportional to some dependency in the particle size (usually square root of particle width) while for the latter, the linear rate of channel propagation rate is proportional to some function of particle size (square of particle diameter for the nickel-catalyzed hydrogenation of graphite). They have envisioned that in a strong oxidizing environment (as in the C-O₂ reaction), after the scission of the carbon-carbon bond by platinum at the graphite-catalyst interface this carbon is dissolved in the particle and diffuses through a viscous outer layer of the particle. At the cooler part of the particle, carbon is converted to either or both carbon dioxide and carbon monoxide by reaction with atomic or molecular oxygen, thereby

creating a carbon concentration gradient within the particle. While in reality this process is seemingly quite complex, consisting of a number of steps, and any of which could be rate determining, we have thought our model which probably could explain Baker's hypothesis.

Here, we have considered a single catalyst particle already creating a channel so that we render devoid the initial transients such as wetting, spreading and agglomeration of particles. Although Baker and co-workers contend a non-isothermal particle, it is regarded here as a first approximation that the particle is isothermal as well as the support (i.e. carbon). The thin viscous (outer) oxide layer is well-established and provides a concentration gradient for carbon within the reduced metal matrix. Carbon diffuses from the catalyst-graphite interface to the top surface. A schematic representation of the process is given in Figure (IV-10). A two-dimensional view of the carbon diffusion is assumed since the particle is moving along the channel's path, i.e., lateral diffusion is small compared to diffusion from the bottom and front. There is no diffusion and reaction of carbon behind the particle. It is assumed that the diffusion coefficients are concentration independent. The thickness of the viscous oxide layer is small and remains constant throughout the steady-state motion of the particle. There is a limiting rate of transport of carbon from the "bulk" metal to the external surface of the particle because of the presence

of a thin viscous oxide layer. This rate is proportional to the difference in concentration of carbon at the metal-viscous metal oxide interface and at the surface. The proportionality "constant" is modeled by using a film theory where such constant is determined by the diffusion coefficient of carbon within the metal oxide and the thickness, δ . The C-O₂ reaction only occurs at the top surface, and when oxygen is in excess, it is assumed that the rate is first order in surface carbon concentration. Since the concentration of carbon is distributed along the horizontal, its rate of consumption on the surface is not uniformly distributed so that both carbon surface concentration gradient and the mobile viscous nature of the oxide layer could impose a surface diffusion of carbon on the surface. Hence, for the metal matrix, the carbon balance equation in dimensionless form is

$$\frac{\partial^2 \hat{c}}{\partial \xi^2} + \frac{\partial^2 \hat{c}}{\partial \zeta^2} = 0 \quad (\text{IV-1})$$

$$\hat{c}(0, \zeta) = 0 \quad (\text{IV-2a})$$

$$\left. \frac{\partial \hat{c}}{\partial \xi} \right|_{\xi=1} = 0 \quad (\text{IV-2b})$$

$$\left. \frac{\partial \hat{c}}{\partial \zeta} \right|_{\zeta=0} = 0 \quad (\text{IV-2c})$$

$$-\left. \frac{\partial \hat{\underline{c}}}{\partial \zeta} \right|_{\zeta=1} + \phi_1 \left[1 - \hat{\underline{c}} \right]_{\zeta=1} - \phi_4 \underline{c}^s = 0 \quad (\text{IV-2d})$$

, where

$$\underline{c} = c/c_0$$

$$\hat{\underline{c}} = 1 - \underline{c}$$

$$\underline{c}^s = c^s/c_0^s$$

c_0 = carbon concentration at the metal-carbon interface

c^s = surface carbon concentration

c_0^s = reference carbon concentration on the surface

$$\xi = x/L, \quad \zeta = y/L \quad (\text{ see Figure IV-11})$$

$$\phi_1 = K_c L / D_{cm}$$

$$K_c = \text{mass transfer coefficient} = \frac{D_{c-mo}}{\delta}$$

D_{cm} = diffusion coefficient of carbon atoms in the metal matrix

D_{c-mo} = diffusion coefficient of carbon atoms in the metal oxide layer

$$\phi_4 = \tilde{k} \left(\frac{D_{c-mo}}{D_{cm}} \right) \left(\frac{c_0^s}{c_0} \right) \left(\frac{L}{\delta} \right)$$

\tilde{k} = a thermodynamic constant relating the surface concentration to the volume concentration in

the metal oxide layer

L = particle size. Here it is assumed, as a first approximation, the particle is cubic.

The surface carbon balance equation in a dimensionless form is given by

$$\frac{d^2 \underline{c}^s}{d \xi^2} - \phi_2^2 \underline{c}^s - \phi_3 \frac{\partial \hat{c}}{\partial \zeta} \Big|_{\zeta=1} = 0 \quad (\text{IV-3})$$

$$\underline{c}^s \Big|_{\xi=0} = \Lambda \quad (\text{IV-4a})$$

$$\frac{d \underline{c}^s}{d \xi} \Big|_{\xi=1} = 0 \quad (\text{IV-4b})$$

, where $\phi_2^2 = \frac{k L^2}{D_{cs}}$

k = first order reaction rate constant

D_{cs} = surface diffusion coefficient on a viscous metal oxide layer

$$\phi_3 = \frac{D_{cm} L C_0}{D_{cs} C_0^s}$$

$$\Lambda = \frac{C^s(0)}{C_0^s}$$

The solution to this set of ordinary-partial differential equations is discussed in detail in Appendix.

Hence, the concentration profile for the carbon atoms in the metal matrix is given by

$$\tilde{c} = 1 - 2 \sum_{n=0}^{\infty} \frac{\left[\frac{\Lambda \tilde{k} c_0^s}{c_0} - 1 \right] \sin \lambda_n \xi \cosh \lambda_n \zeta}{\left[\frac{D_{cm} \tilde{k} L}{D_{cs}} - \frac{D_{cm} k \delta L}{D_{cs} D_{c-mo}} - \frac{\lambda_n^2 D_{cm} \delta}{D_{c-mo} L} \right] \sinh \lambda_n - \lambda_n \cosh \lambda_n}$$

(IV-5)

, where $\lambda_n = \frac{2n+1}{2} \pi$

And the surface carbon concentration is given by

$$\tilde{c}^s = \Lambda \left[\cosh \phi_2 \xi - \tanh \phi_2 \sinh \phi_2 \xi \right] - \phi_3 \sum_{n=0}^{\infty} \frac{\tilde{A}_n \sin \lambda_n \xi}{\phi_2^2 + \lambda_n^2}$$

(IV-6)

, where $\tilde{A}_n = \frac{\lambda_n (2\Lambda \phi_4 - 2\phi_1)}{\phi_3 \phi_4 - \phi_2^2 - \lambda_n^2 - \phi_1 \lambda_n \coth \lambda_n}$

The channel propagation rate is given by

$$\begin{aligned} -\langle v \rangle C_0 &= \text{average flux of carbon at the carbon-} \\ &\quad \text{metal interface} \\ &= \frac{1}{L} \int_0^L N_c \Big|_{x=0} dy \end{aligned}$$

, where $N_c = \text{flux of carbon atoms}$

$$\langle v \rangle = \frac{2}{c_0} \left(c_0 - k \Lambda c_0^s \right) \sum_{n=0}^{\infty} \left[\frac{\hat{k} L^2}{D_{CS}} - \frac{\lambda_n L}{D_{cm} \tanh \lambda_n} - \frac{\lambda_n^2 \delta}{D_{C-mo}} \right]^{-1}$$

(IV-7)

In order to determine the dependency of propagation rate on the particle size, we employed the following physical property data.

$$\begin{aligned} k &= k_0 \exp(-E/RT) \\ &= 10^{13} \exp(-80/1.987 \times 10^{-13} \times 1073) \\ &= 5.06 \times 10^{-4} \text{ sec}^{-1} \end{aligned}$$

Here, $E = 80$ Kcal/mole at 800°C was based on the value obtained by Otto and Shelf (28), and the preexponential factor was taken as 10^{13} sec^{-1} , a typical value for k_0 .

The surface diffusivity of carbon atoms, D_{CS} , was taken from the equation,

$$\begin{aligned} D_{CS} &= 4.7 \times 10^{-2} \exp(-21 \times 10^3/RT) \\ &= 2.5 \times 10^{-6} \text{ cm}^2/\text{sec}, \end{aligned}$$

experimentally obtained by Polak (42) for nitrogen on the (110) plane of tungsten. Due to the lack of the data on the diffusivity of carbon atoms through the metal oxide layer, D_{C-mo} was assumed to be the same as D_{CS} , $2.5 \times 10^{-6} \text{ cm}^2/\text{sec}$.

The diffusivity of carbon atoms within the metal matrix, $D_{cm} = 2 \times 10^{-7} \text{ cm}^2/\text{sec}$, was obtained from the high-temperature vacuum metallographic studies of carbon atom diffusion in metals by L'nyanoi (43).

The solubility of carbon in platinum was assumed to be 10 atom %, based on the data by Ershov (44). The concentration of carbon atoms at the carbon-metal interface, C_O , was calculated from this solubility data using the density of platinum of 21.4 g/ml.

$$\begin{aligned} \text{Volume of 100 platinum atoms} \\ &= \frac{(100 \text{ atoms}) (195.09 \text{ g}/6.02 \times 10^{23} \text{ atoms})}{21.4 \text{ g/ml}} \\ &= 1.51 \times 10^{-21} \text{ cm}^3 \end{aligned}$$

$$\begin{aligned} \text{Hence,} \\ C_O &= \frac{10 \text{ atoms}/6.02 \times 10^{23} \text{ atoms/mole}}{1.51 \times 10^{-21} \text{ cm}^3} \\ &= 1.1 \times 10^{-2} \text{ moles/cm}^3 \end{aligned}$$

Assuming the effective thickness of oxide layer to be 20 Å and knowing the density of carbon atoms of 2.26 g/cm³, $C_O^S = 4.0 \times 10^{-8} \text{ mole/cm}^2$. $\Lambda = C_O/C_O^S$ (at $x=0$) = 1.0, since carbon atoms are likely to be supplied through the metal matrix to the oxide surface efficiently so as to maintain its saturation level at $x = 0$.

A plot of particle velocity (or channel propagation rate) versus particle width is shown in Figure (IV-12). For a fixed k , it is clear that there is an inverse relation between particle velocity and particle width. There is a

striking match between this model for $\tilde{k} = 2.7501 \times 10^5/\text{cm}$ and Baker's data, as shown in Figure (IV-12), both qualitatively and quantitatively. Although their data is for palladium, our model seems to suggest the existence of a thin oxide layer on a metal particle.

Channel Propagation Rate
(nm)

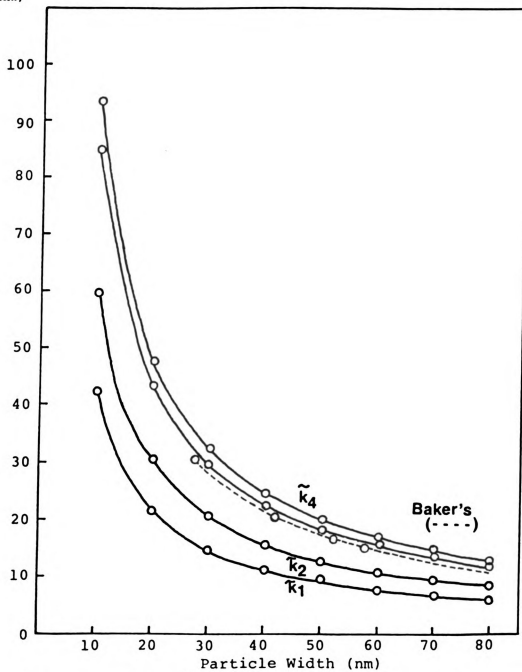


Figure IV-12 $(\tilde{k}_1 = 2.75005 \times 10^5, \tilde{k}_2 = 2.75007 \times 10^5,$
 $\tilde{k}_3 = 2.75010 \times 10^5, \tilde{k}_4 = 2.75011 \times 10^5)$

Channel Propagation Rate
(cm/sec)

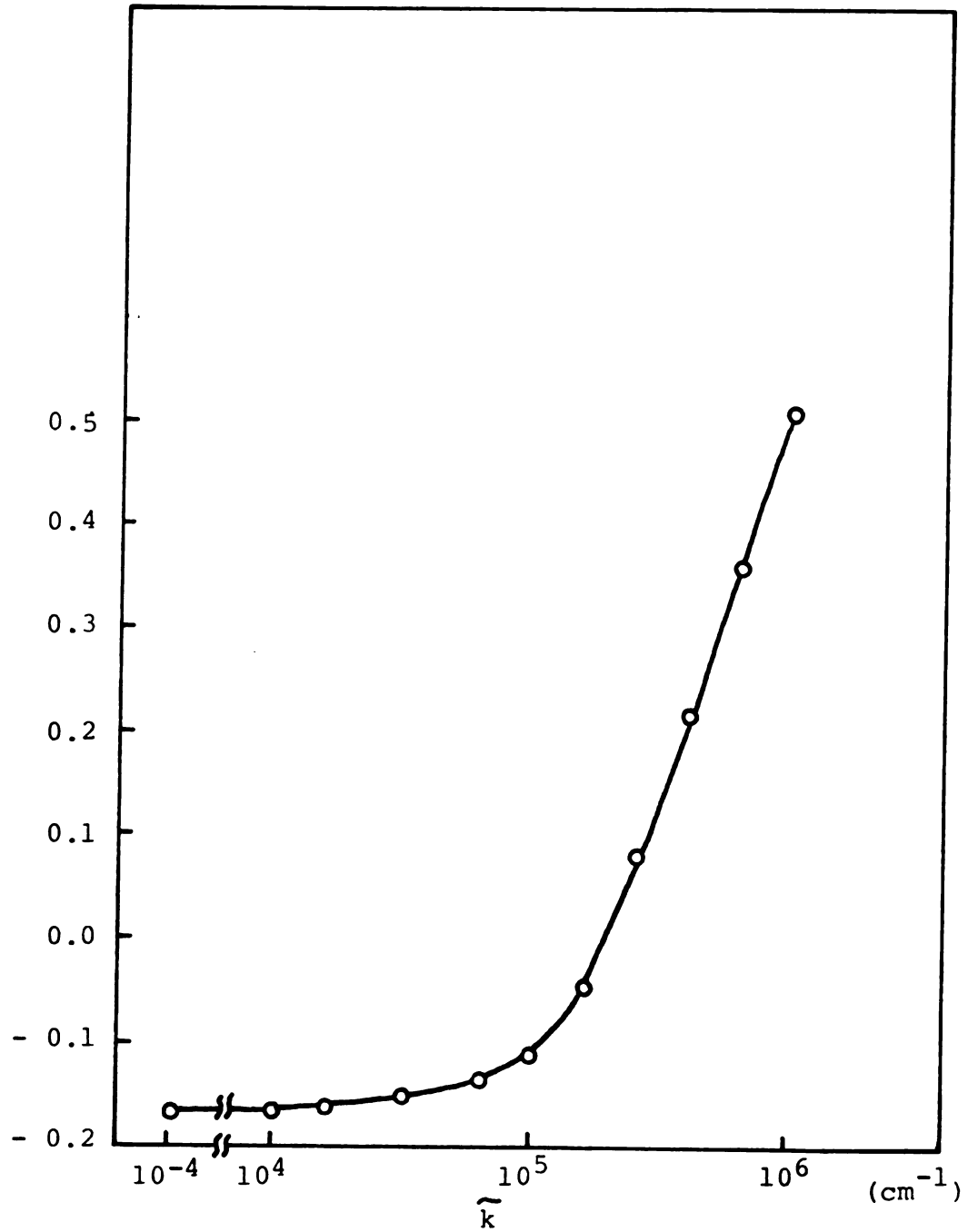


Figure IV-13 Dependency of Propagation Rate
on \tilde{k}

CLOSURES

The kinetics of the oxidation and steam gasification of graphite and platinum graphimet has been presented. The kinetic studies employ temperature programmed desorption/reaction. A scanning transmission electron microscopy of both unreacted and reacted platinum graphimet reveals that the behavior and morphologies are similar to those found by Controlled Atmosphere Electron Microscopy. A correlation using a mathematical model of the temperature programmed desorption/reaction experiments show that platinum increases the density of active sites. This is attributed to the scission of carbon-carbon bonds by platinum. The lowering of the catalyzed oxidation temperature is explained by the scission function of platinum. For platinum, there is some possibility that both electron and oxygen transfer mechanism could be operating for the catalyzed reaction. The latter is suggested by a match between Baker's Controlled Atmosphere Electron Microscopy studies and a simple mathematical model using the assumptions of surface diffusion and viscous oxide layer.

APPENDICES

Appendix A. Computer Program and Sample
Calculations


```

PROGRAM TFD          74/175  OPT=1          FTN 4.2+5E7

1  PROGRAM TFD(INPUT,OUTPUT,TAPE5=INPUT,TAPE6=OUTPUT)
   INTEGER N,METH,MITER,INDEX,INX(27),IER,K
   REAL Y(2),WK(26),X,TOL,XEND,H,EC,EM,HRB,PF,GAMMAC,GAMMA*,
1  EXTERNAL FCN,CONST
   V=5
   Y(1)=1.0
   Y(2)=1.0
10  TOL=0.00001
   H=0.0000001
   METH=2
   MITER=2
   INDEX=1
15  WRITE(6,50)
   EC=260000.
   SK=300000.
   HRB=0.000056
   PI=1.E+13
   GAMMAC=EC/2477.6
   GAMMA=EM/2477.6
20  CONST=PF*EXP((-1.)*GAMMAC)
   CONST=PF*EXP((-1.)*GAMMA)
   SRATIO=5.
   DO 100,K=1,70
   XEND=EC+K*505.1
   CALL DGARCN,FCN,FCNJ,X,H,Y,XEND,TOL,METH,MITER,INDEX,INX,WK,IER)
1  Y(1)=.97128) GO TO 400
   Y(2)=LE=0.D.AND.Y(2).LE=0.0) GO TO 300
   I=1
   Y(1)=LE=1.E-5) Y(2)=0
   I=I+1/SRATIO) GO TO 1
   I=I-1/SRATIO) GO TO 1
   SRATIO=CONST*EXP(GAMMAC)
2  WRITE(6,60)EC,EM,X,Y(1),Y(2),I,OF
35  CONTINUE
   GO TO 400
   Y(1)=0
   Y(2)=0
   TOFF=0
40  WRITE(5,60)EC,EM,X,Y(1),Y(2),I,OF
   STOP
400  FORMAT(1I," E CARBON (J)",3X," E METAL (J)",
50  13," T/TC",10X," CONC",10X," CONM",20X," TURNOVER FREQUENCY",
65  FORMAT(4X,F8.1,7X,F8.1,5X,F4.2,7X,F10.8,4X,F10.8,20X,F10.8)
   END

```

FIN 4.2*

74/175 OPT=1

SUBROUTINE FCV

```

1 SUBROUTINE FCV(N,X,Y,YPRIME)
  INTEGER N
  REAL Y(N),YPRIME(N),X,EC,EM,HRB,PF,GAMMAC,GAMMA,
  1 CONSTC,CONSTM
  EC=26.0000.
  EM=31.0000.
  HRB=.00056
  PF=1.E+17
  GAMMAC=EC/2477.6
  GAMMA=EM/2477.6
  CONSTC=PF*EXP((-1.)*GAMMAC)
  CONSTM=PF*EXP((-1.)*GAMMA)
  YPRIME(1)=-1.*(CONSTC/HRB)*Y(1)*EXP(GAMMAC*(1.-1./X))
  YPRIME(2)=-1.*(CONSTM/HRB)*Y(2)*EXP(GAMMA*(1.-1./X))
  RETURN
  END
10
15

```

74/175 OPT=1

SUBROUTINE FCVJ

```

1 SUPROUTINE FCVJ(N,X,Y,PD)
  INTEGER N
  REAL Y(N),PD(N),X
  RETURN
  END
5

```



```

PROGRAM VELD          74/173  CPY=1          FTW 4.0+537

1  PROGRAM VELD(INPUT,OUTPUT,TAPE=INPUT,TAPE=OUTPUT)
   WRITE(*,20)
   READ(*,10) S
   IF(S.EQ.-1.) GO TO 400
   YLS=1.E-8
   YLE=2.E-7
   DCE=2.E-6
   CCS=2.E-6
   CLAMP=1.
   CGL=1.E-6
   SGN=1.E-7
   ZK=2.75005E+5
   V=0.

10  TSUM=0.
   F1=CN=10.+V+.1)*5.1415725.
   S0=V*(2.-2.+CLAMP)*F1*(C/SGC)/(C*(K/DCS))*XL*2.-E1E/V
   I=(CLM+IAMB*(1-CEH))*XL-EISEH*2*DELTA(L/DCG)
   TSUM=TSUM+SUM
   IF(ABS(SUM).LE.1.E-5) GO TO 200
   V=V+.1.
   GO TO 100.

20  V=TSUM
   WRITE(*,30) XL,V*F
   GO TO 300

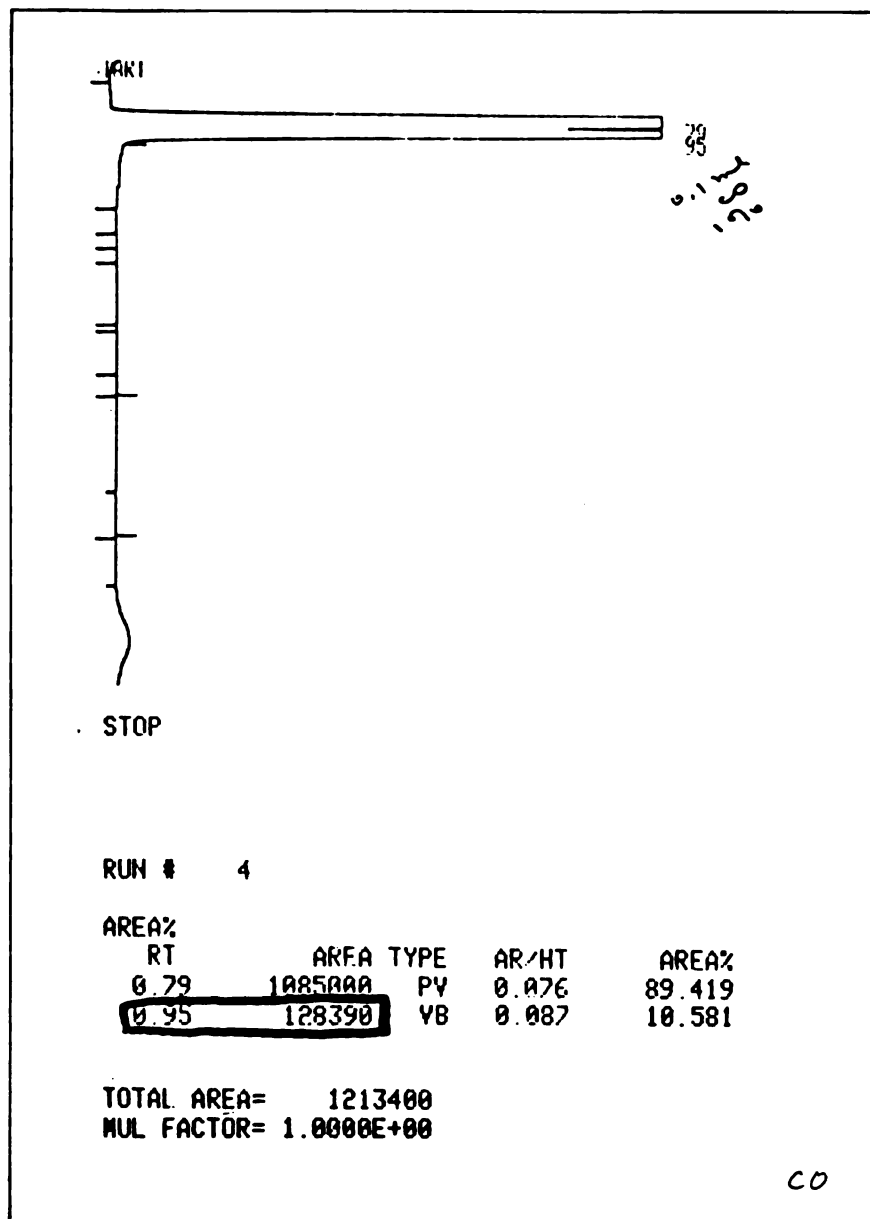
40 1  FORMAT(5G.2)
   2  FORMAT(1G.2)
   3  FORMAT(1X,2E.20,15)
   END

LENGTH          PROPAGATION VELOCITY
.10E-05          .00007493169487E
.20E-05          .00003746584943E
.30E-05          .00002497723302E
.40E-05          .0000179705882
.50E-05          .00000995337917
.60E-05          .0000076244082
.70E-05          .0000066633333E
.80E-05          .0000059064411E

```

Appendix B. Standardization of G. C. Units

A. 0.1 ml of 1% CO standard sample



Since the gas is very dilute,
assume ideal gas behavior.

$$PV = nRT$$

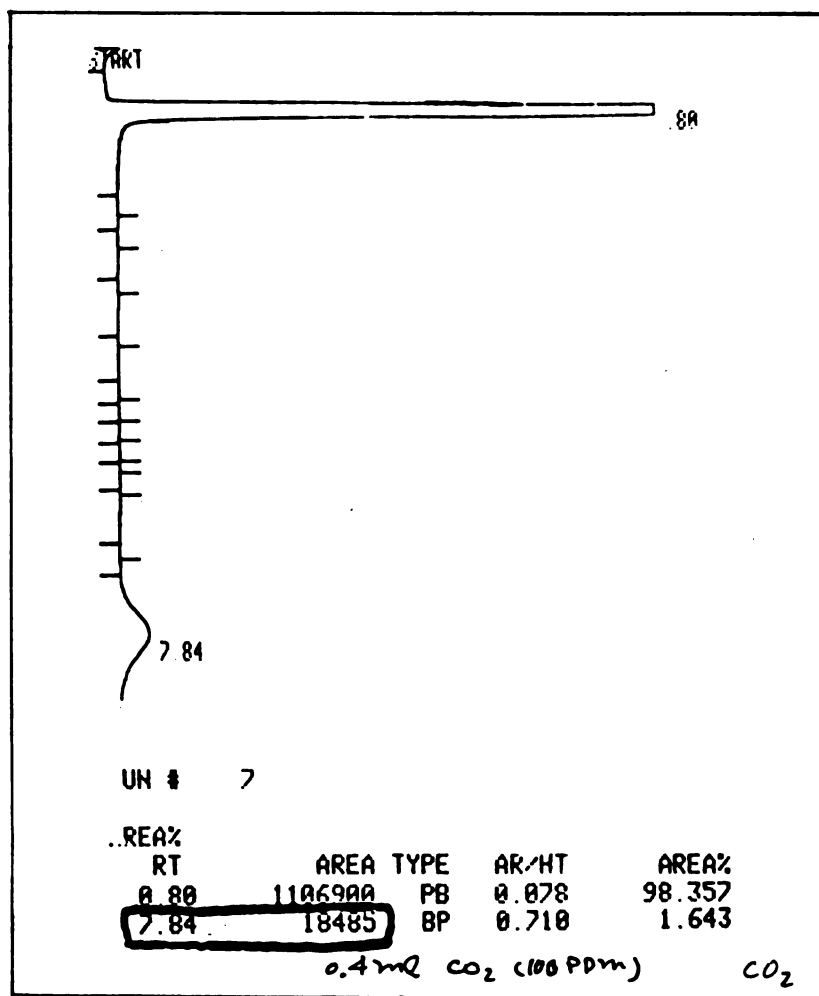
$$(1 \text{ atm}) (0.1 \times 10^{-3} \text{ liter}) (10^2) = n (0.082 \frac{\text{lit atm}}{\text{mole K}}) (298 \text{ K})$$

$$n = 4.092 \times 10^{-8} \text{ moles CO}$$

Hence

$$\text{one unit b.c. reading} = \frac{4.092 \times 10^{-8}}{128390} = 3.187 \times 10^{-13} \text{ moles CO}$$

B. 0.4 ml of 100 ppm CO₂ standard sample



Again, assuming ideal gas,

$$PV = nRT$$

$$(1 \text{ atm})(0.4 \times 10^{-3} \text{ liter})(10^{-4}) = n(0.082 \frac{\text{liter atm}}{\text{mole} \cdot \text{K}})(298^\circ \text{K})$$

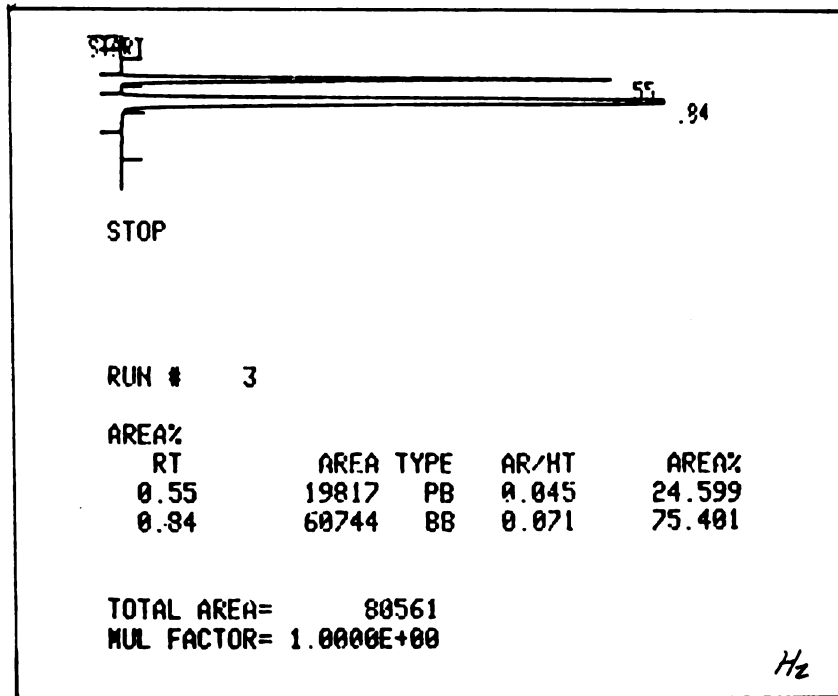
$$n = 1.637 \times 10^{-9} \text{ moles } \text{CO}_2$$

Hence

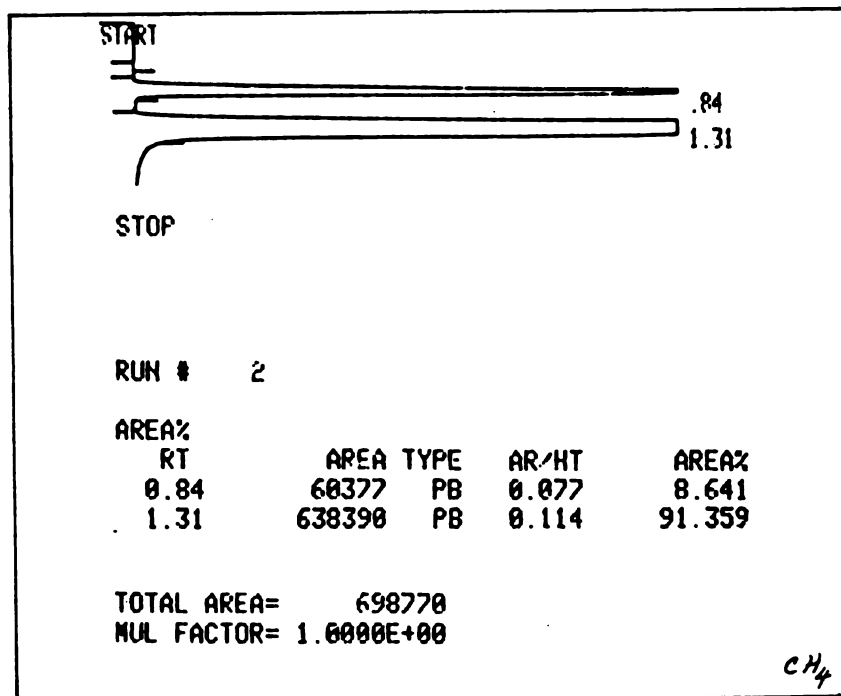
$$\text{one unit O.C. reading} = \frac{1.637 \times 10^{-9}}{18485}$$

$$= 8.855 \times 10^{-14} \text{ moles } \text{CO}_2$$

C. 0.01 ml of 90.5% pure H_2 and
0.01 ml of 99.995% pure CH_4



By the same analogy,
one reading = 1.87×10^{-11} moles H_2



one unit reading = 6.41×10^{-13} moles CH_4

Appendix C. Solutions to Equations (IV-1) to (IV-4)

Solutions to Equations (IV-1) to (IV-4)

$$\hat{c} = X(\xi) Y(\zeta) \quad (A-1)$$

Substitute Equation (A-1) into Equation (IV-1).

$$\frac{X''}{X} = -\frac{Y''}{Y} = -\lambda^2 \quad (\lambda > 0)$$

$$(a) \quad X'' + \lambda^2 X = 0$$

$$X(\xi) = A \sin \lambda \xi + B \cos \lambda \xi$$

Applying Equations (IV-2a) and (IV-2b),

$$X(\xi) = A \sin \lambda_n \xi,$$

$$\lambda_n = \frac{2n+1}{2} \pi, \quad n = 0, 1, 2, \dots$$

$$(b) \quad Y'' - \lambda^2 Y = 0$$

$$Y(\zeta) = A' \sinh \lambda_n \zeta + B' \cosh \lambda_n \zeta$$

Applying Equation (IV-2c),

$$A' = 0$$

$$\text{Hence, } \hat{c}(\xi, \zeta) = \sum_{n=0}^{\infty} A_n \sin \lambda_n \xi \cosh \lambda_n \zeta \quad (A-2)$$

A_n 's will be determined from Equation (IV-2d) after solving the equation for the oxide layer.

$$\left. \frac{\partial \hat{c}}{\partial \zeta} \right|_{\zeta=1} = \sum_{n=0}^{\infty} A_n \lambda_n \sinh \lambda_n \sin \lambda_n \xi$$

$$= \sum_{n=0}^{\infty} \tilde{A}_n \sin \lambda_n \xi$$

$$\text{where } \tilde{A}_n = A_n \lambda_n \sinh \lambda_n$$

Substitute $\frac{\partial \tilde{\zeta}}{\partial \xi} \Big|_{\xi=1}$ into Equation (IV-3).

$$\frac{d^2 \tilde{\zeta}^S}{d\xi^2} - \phi_2 \tilde{\zeta}^S = \phi_3 \sum_{n=0}^{\infty} \tilde{A}_n \sin \lambda_n \xi \quad (A-3)$$

$$\text{Let } \tilde{\zeta}^S = \tilde{\zeta}_h^S + \tilde{\zeta}_p^S$$

$$\tilde{\zeta}_h^S = c_1 \sinh \phi_2 \xi + c_2 \cosh \phi_2 \xi$$

$$= c_1 f_1(\xi) + c_2 f_2(\xi)$$

$$\tilde{\zeta}_p^S = -f_1(\xi) \int \frac{f_1(t) f_2(t)}{W(t)} dt + f_2(\xi) \int \frac{f_2(t) f_1(t)}{W(t)} dt$$

where

$$W(t) = \begin{vmatrix} f_1(t) & f_2(t) \\ f_1'(t) & f_2'(t) \end{vmatrix} = -\phi_2$$

Hence

$$\begin{aligned} \tilde{\zeta}_p^S &= \frac{\sinh \phi_2 \xi}{\phi_2} \int \phi_3 \sum_{n=0}^{\infty} \tilde{A}_n \sin \lambda_n t \cosh \phi_2 t dt \\ &\quad - \frac{\cosh \phi_2 \xi}{\phi_2} \int \phi_3 \sum_{n=0}^{\infty} \tilde{A}_n \sin \lambda_n t \sinh \phi_2 t dt \\ &= \left(\frac{\phi_3}{\phi_2} \right) \sinh \phi_2 \xi \sum_{n=0}^{\infty} \tilde{A}_n \left[\frac{\phi_2 \sinh \phi_2 \xi \sin \lambda_n \xi - \lambda_n \cosh \phi_2 \xi \cos \lambda_n \xi}{\phi_2^2 + \lambda_n^2} \right] \\ &\quad - \left(\frac{\phi_3}{\phi_2} \right) \cosh \phi_2 \xi \sum_{n=0}^{\infty} \tilde{A}_n \left[\frac{\phi_2 \cosh \phi_2 \xi \sin \lambda_n \xi - \lambda_n \sinh \phi_2 \xi \cos \lambda_n \xi}{\phi_2^2 + \lambda_n^2} \right] \\ &= -\phi_3 \sum_{n=0}^{\infty} \frac{\tilde{A}_n \sin \lambda_n \xi}{\phi_2^2 + \lambda_n^2} \end{aligned}$$

$$\tilde{\zeta}^S = c_1 \sinh \phi_2 \xi + c_2 \cosh \phi_2 \xi - \phi_3 \sum_{n=0}^{\infty} \frac{\tilde{A}_n \sin \lambda_n \xi}{\phi_2^2 + \lambda_n^2}$$

Applying Equations (IV-4a) and (IV-4b),

$$\tilde{\zeta}^S(\xi) = \Lambda (\cosh \phi_2 \xi - \tanh \phi_2 \sinh \phi_2 \xi) - \phi_3 \sum_{n=0}^{\infty} \frac{\tilde{A}_n \sin \lambda_n \xi}{\phi_2^2 + \lambda_n^2} \quad (A-4)$$

Now substitute Equations (A-2) and (A-4) into Equation (IV-2d).

Then we have

$$0 = - \sum_{n=0}^{\infty} A_n \lambda_n \sinh \lambda_n \sin \lambda_n \xi + \phi_1 \left(1 - \sum_{n=0}^{\infty} A_n \cosh \lambda_n \sin \lambda_n \xi \right) \\ - \phi_4 \Lambda (\cosh \phi_2 \xi - \tanh \phi_2 \sinh \phi_2 \xi) + \phi_3 \phi_4 \sum_{n=0}^{\infty} \frac{A_n \lambda_n \sinh \lambda_n \sin \lambda_n \xi}{\phi_2^2 + \lambda_n^2}$$

Multiply the equation above by $\sin \lambda_m \xi$ and integrate from $\xi=0$ to $\xi=1$.

$$- \sum_{n=0}^{\infty} A_n \lambda_n \sinh \lambda_n \int_0^1 \sin \lambda_n \xi \sin \lambda_m \xi d\xi + \phi_1 \int_0^1 \sin \lambda_m \xi d\xi \\ - \phi_1 \sum_{n=0}^{\infty} A_n \cosh \lambda_n \int_0^1 \sin \lambda_n \xi \sin \lambda_m \xi d\xi \\ - \phi_4 \Lambda \int_0^1 (\cosh \phi_2 \xi \sin \lambda_m \xi - \tanh \phi_2 \sinh \phi_2 \xi \sin \lambda_m \xi) d\xi \\ + \phi_3 \phi_4 \sum_{n=0}^{\infty} \frac{A_n \lambda_n \sinh \lambda_n}{\phi_2^2 + \lambda_n^2} \int_0^1 \sin \lambda_n \xi \sin \lambda_m \xi d\xi = 0$$

Using the orthogonality.

$$- A_m \lambda_m \sinh \lambda_m \left[\frac{\xi}{2} - \frac{\sin 2\lambda_m \xi}{4\lambda_m} \right]_0^1 + \phi_1 \left[- \frac{\cos \lambda_m \xi}{\lambda_m} \right]_0^1 \\ - \phi_1 A_m \cosh \lambda_m \left[\frac{\xi}{2} - \frac{\sin 2\lambda_m \xi}{4\lambda_m} \right]_0^1 \\ - \phi_4 \left[\frac{\phi_2 \sinh \phi_2 \xi \sin \lambda_m \xi - \lambda_m \cosh \phi_2 \xi \cos \lambda_m \xi}{\phi_2^2 + \lambda_m^2} \right]_0^1 \\ - \tanh \phi_2 \left[\frac{\phi_2 \cosh \phi_2 \xi \sin \lambda_m \xi - \lambda_m \sinh \phi_2 \xi \cos \lambda_m \xi}{\phi_2^2 + \lambda_m^2} \right]_0^1 \\ + \phi_3 \phi_4 \frac{A_m \lambda_m \sinh \lambda_m}{\phi_2^2 + \lambda_m^2} \left[\frac{\xi}{2} - \frac{\sin 2\lambda_m \xi}{4\lambda_m} \right]_0^1 = 0$$

Solve for A_m .

$$A_m = \frac{2\Lambda \phi_4 - 2\phi_1 (\phi_2^2 / \lambda_m^2 + 1)}{\sinh \lambda_m (\phi_3 \phi_4 - \phi_2^2 - \lambda_m^2) - \phi_1 \cosh \lambda_m (\phi_2^2 / \lambda_m + \lambda_m)}$$

Substitute this A_m into Equation (A-2), and note $\xi = 1 - \hat{\xi}$.

Hence, we have

$$\zeta = 1 - \frac{\sum_{n=0}^{\infty} [2\Lambda\phi_4 - 2\phi_1(\phi_2^2/\lambda_n^2 + 1)] \sin \lambda_n \xi \cosh \lambda_n \xi}{\sinh \lambda_n (\phi_3\phi_4 - \phi_2^2 - \lambda_n^2) - \phi_1 \cosh \lambda_n (\phi_2^2/\lambda_n + \lambda_n)} \quad (A-5)$$

Total flux entering the metal-carbon interface

$$N_c^{\pm} = L \int_0^L N_c|_{x=0} dy$$

Average flux

$$\langle N_c \rangle = \frac{1}{L} \int_0^L N_c|_{x=0} dy$$

$$= \frac{1}{L} \int_0^1 -\frac{D_{cm} C_0}{L} \frac{\partial \zeta}{\partial \xi} \Big|_{\xi=0} L d\xi,$$

noting $N_c|_{x=0} = -D_{cm} \frac{\partial c}{\partial x} \Big|_{x=0}$.

$$= \frac{D_{cm} C_0}{L} \frac{\sum_{n=0}^{\infty} [2\Lambda\phi_4 - 2\phi_1(\phi_2^2/\lambda_n^2 + 1)]}{\phi_3\phi_4 - \phi_2^2 - \lambda_n^2 - \phi_1(\cosh \lambda_n)(\phi_2^2/\lambda_n + \lambda_n)}$$

Now $\langle N_c \rangle \vec{i} = -C_0 \langle v \rangle \vec{i}$

$$\langle v \rangle = -\frac{D_{cm}}{L} \frac{\sum_{n=0}^{\infty} [2\Lambda\phi_4 - 2\phi_1(\phi_2^2/\lambda_n^2 + 1)]}{\phi_3\phi_4 - \phi_2^2 - \lambda_n^2 - \phi_1(\cosh \lambda_n)(\phi_2^2/\lambda_n + \lambda_n)} \quad (A-6)$$

Substitute ϕ 's and

note that $\phi_2^2/\lambda_n^2 + 1 = \frac{5 \times 10^4 \times 10^{-12}}{2 \times 10^{-6} \times \lambda_n^2} + 1 \approx 1$

and $\phi_2^2/\lambda_n + \lambda_n \approx \lambda_n$.

Finally,

$$\langle v \rangle = \frac{\sum_{n=0}^{\infty} [2 - 2\Lambda \tilde{k} C_0^S / C_0]}{(\tilde{k}/D_{cs}) L^2 - (\lambda_n/D_{cm} \cdot \tanh \lambda_n) L - (\lambda_n^2/D_{c-m}) \delta}$$

LIST OF REFERENCES

LIST OF REFERENCES

1. Cvetanovic, R.J., and Amenomiya, Y., "Application of a Temperature-Programmed Desorption Technique to Catalyst Studies," *Advan. Catal.* 17, 203 (1967)
2. Cvetanovic, R.J., and Amenomiya, Y., "A Temperature Programmed Desorption Technique for Investigation of Practical Catalysts," *Catal. Rev.* 6, 21 (1972)
3. Gorte, R.J., "Design Parameters for Temperature Programmed Desorption from Porous Catalysts," *J. Catal.* 75, 164 (1982)
4. Hertz, R.K., Kiela, J.B., and Martin, S.P., "Adsorption Effects during Temperature-Programmed Desorption of Carbon Monoxide from Supported Platinum," *J. Catal.* 73, 66 (1982)
5. Foger, K., and Anderson, J.R., "Temperature Programmed Desorption of Carbon Monoxide Adsorbed on Supported Platinum Catalysts," *Appl. Surf. Sci.* 2, 335 (1979)
6. Taylor, J.L., and Weinburg, W.H., "A Method for Assessing the Coverage Dependence of Kinetic Parameters: Application to Carbon Monoxide Desorption from Iridium (110)," *Surface Sci.* 78, 259 (1978)
7. Barton, S.S., and Harrison, B.H., "Surface Studies on Graphite: Desorption of Surface Oxide," *J. Chem. Soc. Faraday Trans. I*, 69, 1039 (1973)
8. Harker, H., Horsley, J.B., and Robson, D., "Active Centres Produced in Graphite by Powdering," *Carbon*, 9, 1 (1971)
9. Mrozowski, S., and Andrew, J.F., "Electron Spin Resonance of Broken Carbon Bonds," *Proc. 4th Carbon Conf.* 207 (Pergamon, Oxford, 1960)
10. Gorte, R., and Schmidt, L.D., "Temperature Programmed Desorption with Reaction," *Appl. Surface Sci.* 3, 381 (1979)
11. Long, F.J., and Sykes, W.J., "Effect of Specific Catalysts on the Reactions of the Steam-C System," *J. Chem. Phys.* 47, 361 (1950)

12. Long, F.J., and Sykes, W.J., "Effect of Specific Catalysts on the Reactions of the Steam-C System," *Proc. Royal Soc. (London)* A215, 100 (1952)
13. Walker, Jr., P.L., Shelef, M., and Anderson, R.A., "Catalysis of Carbon Gasification," in Chemistry and Physics of Carbon, Vol. 4 (P.L. Walker, Jr. ed.), Marcel Dekker, New York, 1968
14. Holstein, W.L., and Boudart, M., "Hydrogenolysis of Carbon and its Catalysis by Platinum," *J. Catal.* 72, 51 (1981)
15. Holstein, W.L., and Boudart, M., "Transition Metal Oxide Catalysed Gasification by Oxygen, Water, and Carbon Dioxide," *Fuel*, 62, 162 (1983)
16. Baker, R.T.K., France, J.A., Rouse, L., and Waite, R.J., "Catalytic Oxidation of Graphite by Platinum and Palladium," *J. Catal.* 41, 22 (1976)
17. Baker, R.T.K., Sherwood, R.D., "Catalytic Gasification of Graphite by Nickel in Various Gaseous Environments," *J. Catal.* 70, 198 (1981)
18. Baker, R.T.K., Harris, P.S., Kemper, D.J., and Waite, R.J., "Controlled Atmosphere Electron Microscopy Studies of Graphite Gasification - 3. The Catalytic Influence of Molybdenum and Molybdenum Trioxide," *Carbon* 12, 179 (1974)
19. Baker, R.T.K., and Harris, P.S., "Controlled Atmosphere Electron Microscopy Studies of Graphite Gasification - I. Catalytic Influence of Zinc," *Carbon* 14, 25 (1973)
20. Baker, R.T.K., and Chludzinski, Jr., J.J., "Catalytic Gasification of Graphite by Chromium and Copper in Oxygen, Steam, and Hydrogen," *Carbon* 19, 75 (1981)
21. Keep, C.W., Terry, S., and Wells, M., "Studies of the Nickel-Catalyzed Hydrogenation of Graphite," *J. Catal.* 66, 451 (1980)
22. Blakely, J.P., and Overholster, L.G., "Oxidation of ATJ graphite by Low Concentrations of Water Vapor and Carbon Dioxide in Helium," *Carbon* 3, 269 (1965)
23. Bond, G.C., Catalysis by Metals (Academic Press, New York, 1962)

24. Feates, F.S., and Keep, C.W., "Surface Complexes formed by Thermal and Radiolytic Adsorption of Gases on Graphite," *Trans. Faraday Soc.*, 66, 3156 (1970)
25. Thomas, J.M., *Chemistry and Physics of Carbon*, Vol. 1, 122 (P.L. Walker, Jr., ed.), Marcel Dekker, New York, (1965)
26. Heintz, E.A., and Parker, W.E., "Catalytic Effect of Major Impurities on Graphite Oxidation," *Carbon* 4, 473 (1966)
27. Winicur, D.H., "CO Desorption and Adsorption on Pt (111)," *Surface Sci.* 109, 263 (1981)
28. Otto, K., and Shelef, M., "Catalytic Steam Gasification of Graphite-Effects of Intercalated and Externally Added Ru Rh, Pd and Pt," *Carbon* 15, 317 (1977)
29. Lalancette, J.M., U.S. Patent No. 3, 847, 963, dated November 12, 1974
30. Alfa Division, Ventron Corporation Sales Catalog, p. 451 (1977-1978)
31. Otto, K., and Shelef, M., 6th Int. Congr. Catalysis, London, 1976, Paper B47.
32. McKee, D.W., "The Catalyzed Gasification Reactions of Carbon," in *Chemistry and Physics of Carbon* (P.L. Waler, Jr., and P.A. Throrer, eds.) 16, 1 (1981), Marcel Dekker, Inc., New York.
33. Feates, F.S., Harris, P.S., and Reuben, G.B., "Compensation Effect in the Kinetics of the Catalyzed Oxidation of Carbon," *J. Chem. Soc. Faraday Trans. I*, 70, 2011 (1974)
34. Hennig, G.R., "Catalytic Oxidation of Graphite," *J. Inorg. Nucl. Chem.* 24, 1129 (1962)
35. Presland, A.E.B., and Headley, J.A., "Electron-Microscope Study of the Thermal Oxidation of Natural Graphite," *J. Nucl. Mater.* 10, 99 (1963)
36. L'Homme, G.A., Boudart, M., and D'Or, L., "Kinetic Study of Slow Oxidation of Channel Black by Gaseous Oxygen," *Acad. Roy. Belg. Bull. Cl. Sci.* 5 ser 52, 1249 (1966)

37. McKee, D.W., "Metal Oxides as Catalysts for the Oxidation of Graphite," *Carbon* 8, 623 (1970)
38. Smith, D.J., Fisher, R.M., and Freeman, L.A., "High-Resolution Electron Microscopy of Metal-Intercalated "Graphimets"," *J. Catal.* 72, 51 (1981)
39. Magne, P., and Duval, X., "Existence of Four Types of Reactive Sites in Graphite Oxidation," *Bull. Soc. Chim. Fr.*, A5, 1593 (1976)
40. Marsh, H., and Adair, R.R., "Catalytic Gasification of Doped Carbon-A Kinetic Study," *Carbon* 13, 327 (1975)
41. Buch, T., Guala, J.A., and Caverio, A., "Oxyreactivity of Doped Sucrose Carbon," *Carbon* 16, 377 (1978)
42. Polak, A., and Ehrlich, G., "Surface Self-Diffusion," *J. Vac. Sci. Technol.* 14, 407 (1977)
43. L'nyanoi, V.N., "Determination of the Solid Solution-Graphite Interfacial Energy in Nickel-Carbon, Cobalt-Carbon, and Iron-Carbon Alloys," *Fiz. Khim. Obrab. Mater.* 3, 104 (1977)
44. Ershov, G.S., and Kasatkin, A.A., "Effect of the Alloying Elements on the Viscosity of Liquid Iron and Steels," *Stal'*, 8, 712 (1977)